

Inflight Performance of Cassini Reaction Wheel Bearing Drag in 1997–2013

Allan Y. Lee¹ and Eric K. Wang²

Jet Propulsion Laboratory, California Institute of Technology

Pasadena, CA 91109-8099

As the first spacecraft to achieve orbit at Saturn in 2004, Cassini has collected science data throughout its four-year prime mission (2004–08), and has since been approved for a first and second extended missions through September 2017. Cassini is a three-axis stabilized spacecraft. It uses reaction wheels to achieve high level of spacecraft pointing stability that is needed during imaging operations of several science instruments. The Cassini flight software makes in-flight estimates of reaction wheel bearing drag torque and made them available to the mission operations team. These telemetry data are being trended for the purpose of monitoring the long-term health of the reaction wheel bearings. Anomalous drag torque signatures observed over the past 15 years are described in this paper. One of these anomalous drag conditions is bearing cage instability that appeared (and disappeared) spontaneously and unpredictably. Cage instability is an uncontrolled vibratory motion of the bearing cage that can produce high-impact forces internal to the bearing that will cause intermittent and erratic torque transients. Characteristics of the observed cage instabilities and other drag torque “spikes” are described in this paper. In day-to-day operations, the reaction wheels’ rates must be neither too high nor too low. To protect against operating the wheels in any undesirable conditions (such as prolonged low spin rate operations), a ground software tool named Reaction Wheel Bias Optimization Tool (RBOT) was developed for the management of the wheels. Disciplined and long-term use of this ground software has led to significant reduction in the daily consumption rate of the wheels’ low spin rate dwell time. Flight experience on the use of this ground software tool as well as other lessons learned on the management of Cassini reaction wheels is given in this paper.

Acronyms

AACS	Attitude and Articulation Control (an engineering subsystem)
CCW	Counter-Clockwise
CI	Cage Instability
CW	Clockwise
DFPW	Downlink, Fields, Particles, and Waves (a science mode)
DOY	Day of Year
DSP	Defense Support Program
EHD	Elasto-Hydro-Dynamic
FP	Fault Protection
FSDS	Flight Software Development System (a Cassini software test bed)
FUSE	Far Ultraviolet Spectroscopic Explorer, 2001
GSW	Ground Software
IRU	Inertial Reference Unit
NAC	Narrow Angle Camera
ORS	Optical Remote Sensing (a science mode)
PD	Proportional and Derivative (a controller)
PI	Proportional and Integral (an estimator)
RBOT	RWA Bias Optimization Tool

¹Section Staff, Guidance and Control Section. Division of Autonomous Systems. Mail Stop 230-104, 4800 Oak Grove Drive, Pasadena, CA 91109-8099, USA. Allan.Y.Lee@jpl.nasa.gov.

²Member of Technical Staff, Guidance and Control Flight Software Validation Section. Division of Autonomous Systems. Mail Stop 230–104, 4800 Oak Grove Drive, Pasadena, CA 91109-8099, USA. Lead engineer, Cassini AACS Flight Software. Eric.K.Wang@jpl.nasa.gov.

RCS	Reaction Control System
RHM	Reaction Wheel Hardware Manager
rpm	Revolutions Per Minute
RSS	Root Sum (of) Squares
RWA	Reaction Wheel Assembly
RWAC	Reaction Wheel Controller
S/C	Spacecraft
TIMED	Thermosphere Ionsphere Mesosphere Energetics and Dynamics Spacecraft
XMM	X-ray Multi-mirror Mission, an ESA mission, also called XMM-Newton

Nomenclatures

c	=	Viscous coefficient of the wheel bearing lubrication system, Nms/rad
E	=	Effective Young's modulus of the bearing contacting surface materials, N/m ²
$G(\omega)$	=	A function of wheel spin rate ω defined in Eq. (6), unitless
h_{min}	=	Minimum bearing lubricant film thickness, m
I_{RWA}	=	Moment of inertia of each reaction wheel rotor, kg-m ²
K_I	=	Integrator gain of the RWA drag torque estimator, kg-m ² /s ²
K_P	=	Proportional gain of the RWA drag torque estimator, kg-m ² /s
kPa	=	kilo-Pascal (1 kPa \approx 0.14503 psia)
L^{-1}	=	Inverse Laplace operator
p	=	An exponent of the bearing spin rate defined in Eq. (5) ($p = 0.68-0.73$), unitless
R_E	=	Effective radius of curvature of the two bearing contacting surfaces, m
R_P	=	Pitch radius of the reaction wheel bearing, m
s	=	Laplace variable, rad/s
T_D	=	Dahl drag torque of reaction wheel bearing system, N-m
T_{Drag}	=	Total drag torque of reaction wheel bearing system, N-m
ω	=	Angular rate of the reaction wheel, rad/s (or rpm)
ω_D	=	Bandwidth of the RWA drag torque estimator, rad/s
ζ_D	=	Damping ratio of the RWA drag torque estimator, unitless
Ω_0	=	Initial wheel spin rate of coast-down test, rad/s
τ	=	Time constant of the RWA speed decay (see Eq. (4)), s
η	=	Nominal viscosity of the lubricant used in RWA bearings, Ns/m ²

I. Cassini/Huygens Mission and the Attitude Control System

As the first spacecraft to achieve orbit at Saturn in 2004, Cassini has collected science data throughout its four-year prime mission (2004–08), and has since been approved for a first and second extended missions through September 2017. Major science objectives of the Cassini mission include an investigation of the configuration and dynamics of Saturn's magnetosphere, the structure and composition of the rings, the characterization of several of Saturn's icy satellites, and the constituent abundance of the atmosphere of Titan.¹

A sophisticated interplanetary spacecraft, Cassini is one of the largest spacecraft humans have ever built and launched. The orbiter is about 6.8 m in height with a "diameter" of 4 meters. The total mass of the spacecraft at launch was approximately 5,574 kg. The Cassini Attitude and Articulation Control System (AACS) estimates and controls the attitude of the three-axis stabilized Cassini spacecraft. The AACS responds to ground-commanded pointing goals for the science instruments. To point to the commanded targets within the required accuracy, AACS uses either thrusters or reaction wheels to control the spacecraft's attitude. Attitude determination sensors used by Cassini AACS include two Stellar Reference Units (i.e., star trackers), two Sun Sensor Assemblies, and two Inertial Reference Units (IRU, or gyroscopes).¹

A high level of spacecraft pointing stability is needed during imaging operations of high-resolution science instruments such as the Narrow Angle Camera.²⁻³ Typically, the required level of pointing stability is not achievable with the spacecraft controlled by thrusters. Instead, three Reaction Wheel Assemblies (RWAs) are employed to suit this purpose. Cassini carries a set of three reaction wheels (RWA-1 to RWA-3) that are mounted on the lower equipment module. There is a "backup" wheel that is mounted on top of

an articulation platform.¹ The orientation of the four RWA relative to the spacecraft's coordinate frame (at launch) is depicted in Fig. 1.

Each Cassini reaction wheel uses two R10-size ball bearings that are spring preloaded. The bearings contain a crimped stainless steel ribbon cage, and they are lubricated with light ester oil.¹ Each bearing has metal shields to help prevent oil loss. The wheel units were shielded with an atmosphere of helium gas to retard oil evaporation within their housings. With the helium atmosphere, evaporative loss of lubricant is likely at a minimum. Each wheel carries two platinum thermistors, one in the electronics box and the other in the wheel mechanism. Inflight, all operating wheels' temperatures are maintained within the range of 11–29 °C.

At launch on 15 October 1997, RWA-1 to RWA-3 formed the prime wheel set. First use of the RWA to control the spacecraft attitude was made on 16 March 2000, several months ahead of the start of the Jupiter observation campaign. This prime wheel set was used until 11 July 2003. In October 2002, mission operation team observed anomalous drag torque in the bearing(s) of RWA-3 (see Section IV). A decision was made in mid-2003 to move the articulation platform so as to align RWA-4 with the degraded RWA-3.¹ After 11 July 2003, the prime reaction wheel set became RWA-1, RWA-2, and RWA-4. This prime wheel set has been used from July 2003 to date.

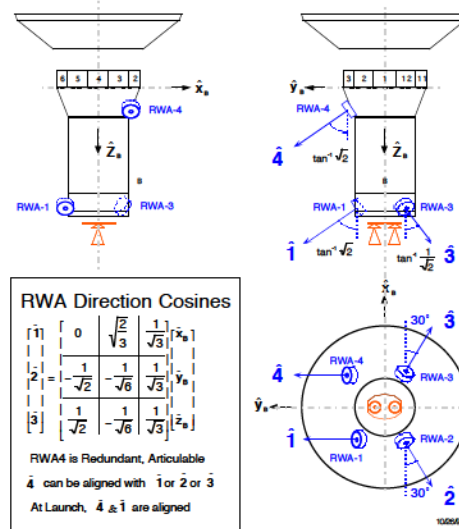


Figure 1. Cassini Reaction Wheel Locations and Orientations^{1,2}

Many spacecraft with attitude controlled by reaction wheels (or control moment gyroscopes) have encountered anomalous wheel bearing drag torque. Some of these bearing-related flight anomalies were fatal. Observed nominal and anomalous flight performance of the Cassini RWA bearing systems are given in this paper. Over the past fifteen years (1997–2012), in “flying” the Cassini spacecraft, the Cassini mission operation team has acquired some useful flight experience on good ways to manage the reaction wheels. These flight lessons learned are also given in this paper.

II. Cassini Reaction Wheel Controller Design²

The reaction wheel assemblies are used primarily for attitude control when precise and stable pointing of a science instrument is required during the prime mission phase. Because the spacecraft's principle axes are very closely aligned with the spacecraft's mechanical axes, the basic structure of the Reaction Wheel Attitude Control System (RWAC) is a decoupled, three-axis, Proportional and Derivative (PD) controller. Fig. 2 is an illustration of the RWAC design.² Cassini pointing stability requirements and flight performance are given in Refs. 2–3.

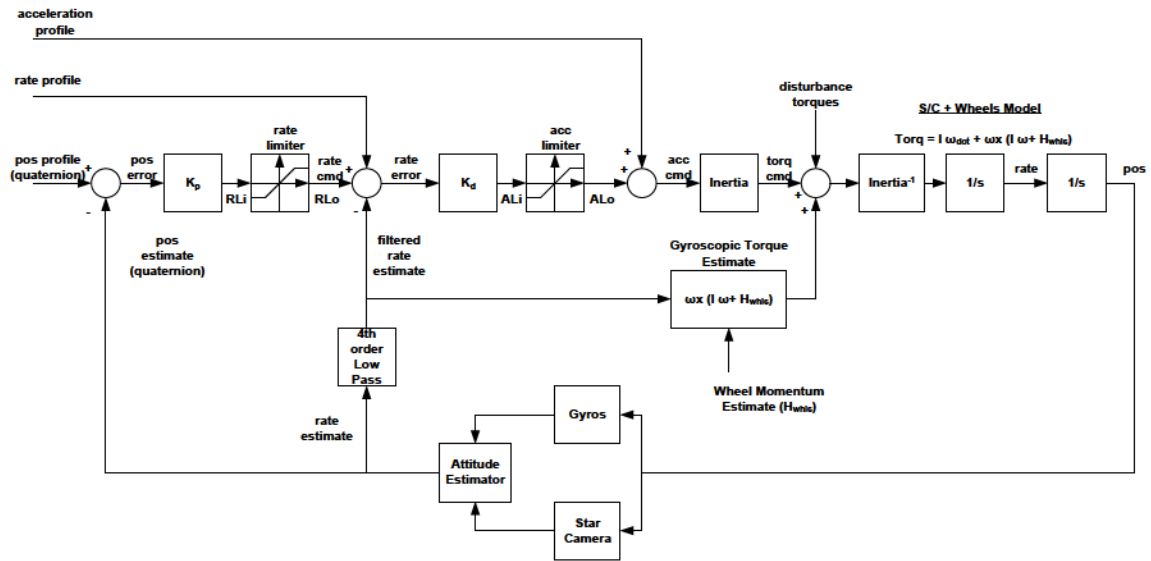


Figure 2. Block Diagram of the Reaction Wheel-based Attitude Control System²

Due to the presence of bearing drag torque in the reaction wheels, a controller with the “PD” control architecture will not be able to drive the spacecraft attitude control error to zero unless an integral term is added to the PD controller. This difficulty was overcome by the addition of a Proportional and Integral (PI) estimator of the bearing drag torque in a flight software object named RWA Hardware Manager (RHM). In effect, integral control action is added “locally” to remove any steady-state spacecraft’s attitude control errors. Fig. 3 is a simplified illustration of the drag torque estimator design. The bandwidth of the drag torque estimator design is 0.01 Hz.^{1,3-4}

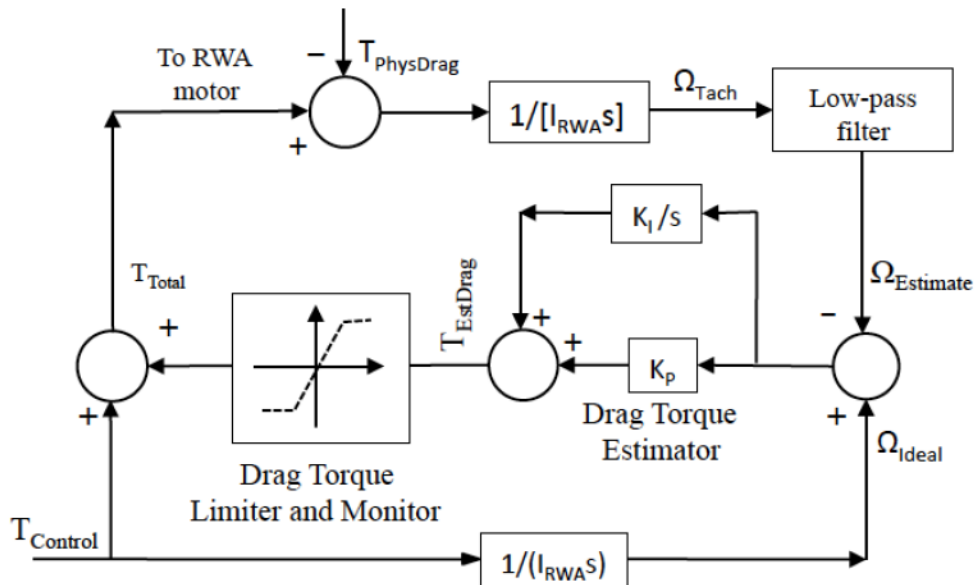


Figure 3. Block diagram of the reaction wheel hardware manager design (adapted from Ref. 4)

A key function performed by the RWA hardware manager is to provide an estimate of the bearing drag torque. As illustrates in Fig. 3, the estimated bearing drag torque will first be “limited” and then added to the S/C’s attitude control torque ($T_{Control}$) to form the total torque command (T_{Total}) that is sent to the RWA

direct current motor. With this drag torque compensation system, if the bearing drag torque is elevated due to anomalous bearing performance, a larger motor torque command will be sent. As a result, impacts of the anomalous bearing drag on the S/C attitude control performance is minimized.

As depicted in Fig. 3, a limiter is placed immediately after the PI drag torque estimator. This will prevent unreasonably large drag torque estimates from being sent to the D.C. motor. At launch, the threshold of the limiter for each wheel is set at 50% higher than the largest ground-measured drag for that wheel. About ten years after launch, these limiters' thresholds were raised in response to observed higher drag torque levels (see Section V). Before being "limited", the raw drag torque estimates feed a set of error monitors named "Excessive RWA Drag Torque". In these error monitors, the drag torque estimates are compared with a set of drag thresholds (determined using ground-based test results, see also Section III). Results from these comparisons, when corroborated with outputs from other error monitors (e.g., the S/C attitude control error monitors) are used to initiate appropriate Fault Protection (FP) responses. The drag estimates are also made available via telemetry to the mission operations team. Ground operators trend this and other data (as well as other telemetry such as the RWA temperatures) to monitor the long-term health of the reaction wheels.

The drag torque estimator was designed to accurately track the physical bearing drag torque only in the steady state. When the physical drag torque changed due to varying RWA spin rate, the drag estimator can still track the physical drag torque but there will be a tracking error. Let $T_{\text{Phy}}(s)$ and $T_{\text{Est}}(s)$ be the transfer functions of the physical and estimated drag torques, respectively. With reference to Fig. 3, it can be shown that:

$$\frac{T_{\text{Est}}(s)}{T_{\text{Phy}}(s)} = \frac{K_p s + K_I}{I_{\text{RWA}} s^2 + K_p s + K_I} = \frac{2\zeta_D \omega_D s + \omega_D^2}{s^2 + 2\zeta_D \omega_D s + \omega_D^2} \quad (1)$$

In this expression, K_p and K_I are the gains of the PI drag torque estimator, and I_{RWA} is the moment of inertia of each reaction wheel's rotor. The gains are selected to be: $K_p = 2\zeta_D \omega_D I_{\text{RWA}}$ and $K_I = \omega_D^2 I_{\text{RWA}}$. Here, ω_D and ζ_D are the bandwidth and damping ratio of the drag torque estimator design ($\omega_D = 0.01$ Hz and $\zeta_D = 0.707$). As an example, Fig. 4 depicts the time history of the estimated drag torques $T_{\text{Est}}(t)$ (in blue solid line) in response to two "triangular impulse" drag torques $T_{\text{Phy}}(t)$ (in red dashed line). Both impulses rise from the nominal drag level to a peak drag level of 2.5 mNm in 10 s. Then, the first and second drag impulses fall from their respective peaks to the nominal level in 10 and 30 s, respectively. As depicted in Fig. 4, the peak levels of the resultant estimated drag torques are 0.6–1.2 mNm, and their "settling" times are 70–80 s. In Section V, observed drag torque "spikes" with symptoms that resemble these estimated drag torques will be discussed.

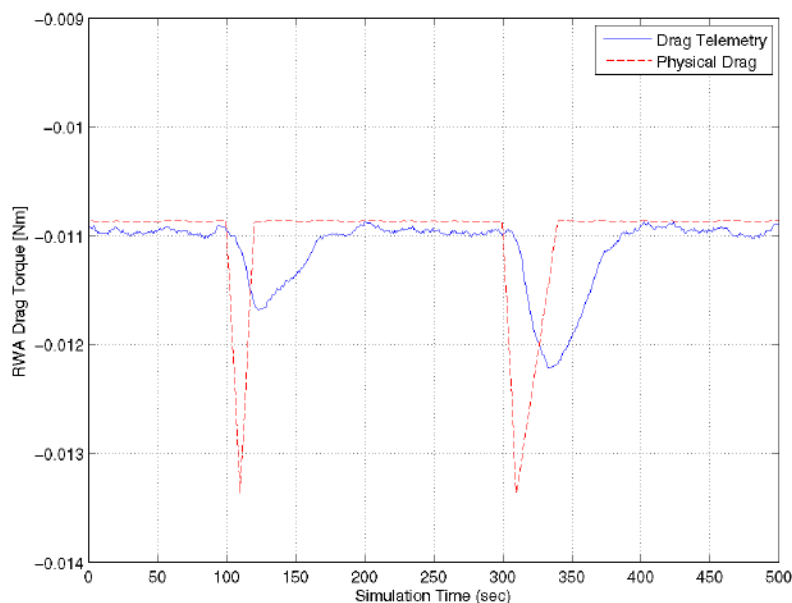


Figure 4. Time histories of estimated RWA drag torques

III. Inflight Calibrations of RWA Drag Performance

In Ref. 5, on-orbit anomaly records for satellites launched from 1990 through 2001 were reviewed to determine trends of space mission critical failures. Anomalies categorized by subsystems showed that the Guidance, Navigation, and Control (GN&C) subsystems have the highest share of anomalies that resulted in critical mission failure. Among all the GN&C equipment failures, the largest number is attributed to wheel failures. Most of these reaction wheel failures are related to anomalous tribological performance of wheel bearings. Hence, the performance of the reaction wheels' bearings should be carefully characterized and trended inflight. This is especially true for long missions such as the Cassini/Huygens mission.

In-flight, the Cassini RWAs were required to be "exercised" every 90 ± 10 days, and characterized every 180 ± 21 days.¹ The first "exercise" of the Cassini wheels was conducted on Launch+15 days. All four wheels were first commanded to be in a "rate control" mode and ran up to +100 rpm. They were then commanded to the "coast" control mode (i.e., removal of all RWA motor torque), and allowed to run down for several minutes. Next, the wheels were again commanded to be in the "rate control" mode and ran up to -100 rpm. After another transition to the "coast" mode, they were again allowed to coast down. On the ground, the RWA rate, RWA rate control error, and other telemetry were analyzed and the performance of the RWA rate control mode was found to be nominal.

Inflight, the bearing performance of all the wheels are characterized via similar coast-down tests. In these tests, the reaction wheels were first commanded to their initial spin rates (e.g., 900 rpm) and were allowed to "coast" down under the action of only the bearing drag torque. One way to model the RWA bearing drag is to use the following linear model:

$$T_{\text{Drag}}(\omega) = -c\omega - T_{\text{Dahl}}\text{sgn}(\omega) \quad (2)$$

Here, c (in Nms/rad) is the viscous coefficient of the wheel bearing lubrication system, ω is the angular rate of the wheel (in rad/s), $\text{sgn}(\omega)$ is the signum function, and T_{Dahl} is a constant Dahl friction parameter. Dahl friction is similar to Coulomb friction. However, reaction wheel bearings do not exhibit the classical stick/slip phenomena of Coulomb friction. Rather, they ramp up to the steady-state Coulomb level exponentially with an "angle" constant of a few degrees of the wheel rotation.⁶ The use of this particular drag torque model is limited to spin rate $|\omega| \geq \omega_{\text{Boundary}}$, where ω_{Boundary} is the spin rate at which the bearing entered the "boundary lubrication" condition (cf. see Section III). Based on observed drag torque telemetry data of the Cassini wheel bearings, an "educated" guess of ω_{Boundary} is about 250 rpm (see also Fig. 5). Many other bearing drag torque models have also been proposed in the literature.⁷

Using the linear drag model, the RWA spin rate is governed by the following differential equation during a coast-down test:

$$I_{\text{RWA}}\dot{\omega}(t) = -c\omega - T_{\text{Dahl}}\text{sgn}(\omega) \quad (3)$$

Here, I_{RWA} is the moment of inertia of the RWA rotor about its spin axis. If $\omega = +\Omega_0$ at time $t = 0$, the solution of Eq. (3) is:

$$\omega(t) = -\frac{T_{\text{Dahl}}}{c}\text{sgn}(\omega) + \left\{ \Omega_0 + \frac{T_{\text{Dahl}}}{c}\text{sgn}(\omega) \right\} e^{-\frac{t}{\tau}} \quad (4)$$

Here, the time constant of the RWA speed decay, τ , is given by I_{RWA}/c . Given the time history $\omega(t)$ of the RWA spin rate, one can determine both the viscous coefficient and the Dahl friction that best fit it. These flight results should then be compared with those determined via similar pre-launch ground tests. Ground test results yielded a mean viscous coefficient of 1.03×10^{-4} Nms/rad and a mean Dahl friction of 4.48×10^{-4} Nm for the four wheels (in both the clockwise and counter-clockwise wheel rotations).

The in-flight coast-down characterization tests involved commanding the wheels to speeds of $+\Omega_0$, $+\Omega_0$, $-\Omega_0$, and $-\Omega_0$, for RWA-1 to RWA-4, respectively (a typical value of $+\Omega_0$ is 900 rpm, see also Table 1). The initial speeds of RWA-1 and RWA-2 are identical (both are in the clockwise direction). Those for RWA-3 and RWA-4 are also identical but they are in the counter-clockwise direction. In this way, the reaction torques imparted on the spacecraft due to the (decaying) RWA drag torques will approximately cancel each other (the geometry of the RWA configuration is such that an exact cancellation is impossible). During these coast-down tests, attitude control thrusters are used to maintain the commanded Earth-pointed attitude of the spacecraft in the presence of any residual unbalanced drag torque imparted on the S/C. The wheel rate pattern stated above $[+\Omega_0, +\Omega_0, -\Omega_0, -\Omega_0]$ will minimize the hydrazine cost and the ΔV imparted on the spacecraft due to these thruster firings. After a predicted coast-down time, the reaction wheels were commanded to $-\Omega_0, -\Omega_0, +\Omega_0$, and $+\Omega_0$ (for RWA-1 to RWA-4, respectively) in order to characterize the

wheel drag performance when they are spun in the opposite direction. All RWA coast-down tests performed inflight are listed in Table 1. From 1999-DOY-025 to 2009-DOY-291 (3,916 days), there were 44 coast-down tests performed for the prime RWA. That is, on the average, a coast-down test was performed every 89 days. The frequency requirement of RWA bearing characterization test (180 days) is met.

Table 1. Cassini RWA Drag Torque Characterization Tests

Year	Days of Year for RWA-124 Tests	Days of Year for RWA-3 Tests	Comments
1999	025, 078, 139, 249, 353		RWA-1234 coast-down initial tests with rates used: ± 836 and ± 418 rpm
2000	143, 272, 354		
2001	179, 190		
2002	005, 024, 032, 094, 187, 221, 295		RWA-1234 coast-down tests with initial rates: ± 900 rpm.
2003	014, 026, 079, 140, 250, 354		First test was performed with [-739, -537, -547] rpm only for RWA-123. All others were performed with initial rates of ± 900 rpm.
2004	137, 139, 243	138, 256	RWA-124 coast-down tests with initial rates of ± 900 rpm.
2005	052, 244	052, 244	
2006	021, 089, 149, 238, 319	026, 153, 307	
2007	042, 121, 210, 299	106, 301	RWA-3 coast-down tests were performed separately with initial rates of ± 600 rpm
2008	029, 110, 170, 288	097, 267	
2009	017, 115, 291 (last test)	051	

A set of (RWA-3) telemetry data observed in a representative coast-down test is depicted in Fig. 5. This coast-down test was performed on 2001-DOY-179. The RWA-3 was commanded to ± 836 rpm and then was allowed to coast down under the action of the bearing drag. Note that the RWA spin rate decayed “smoothly” from 836 rpm until the spin rate fell below 250 rpm. At 250 rpm, one noted an abrupt increase in drag causing the spin rate to decay quickly to zero. It is conjectured that the bearings, when operating with spin rate that is below 250 rpm, had entered a boundary lubrication condition with metal-to-metal contacts between the balls and the races. In this regime, the physics of the drag torque is too complex to be modeled by Eq. (2).

The fatigue life of bearings is greatly extended if there is a continuous presence of lubricant film between the balls/races and between the balls/cage. This could be achieved if the bearing rate is maintained above a certain level. Else, the bearings will enter a sub-EHD (elasto-hydro-dynamic) boundary lubrication state with the thickness of the lubrication film smaller than the root-mean-square values of the surface roughness of the balls and the races. When that happens, there will be metal-to-metal contact between the balls and the races. The high shear stress resulting from these direct contacts will cause an increase in bearing drag torque. These contacts will also promote excessive wear of the balls, cage, and the races. The resultant overheating and polymerization of lubricant will lead to subsequent bearing failure. Obviously, it is undesirable to operate the bearings in this low spin rate sub-EHD state.

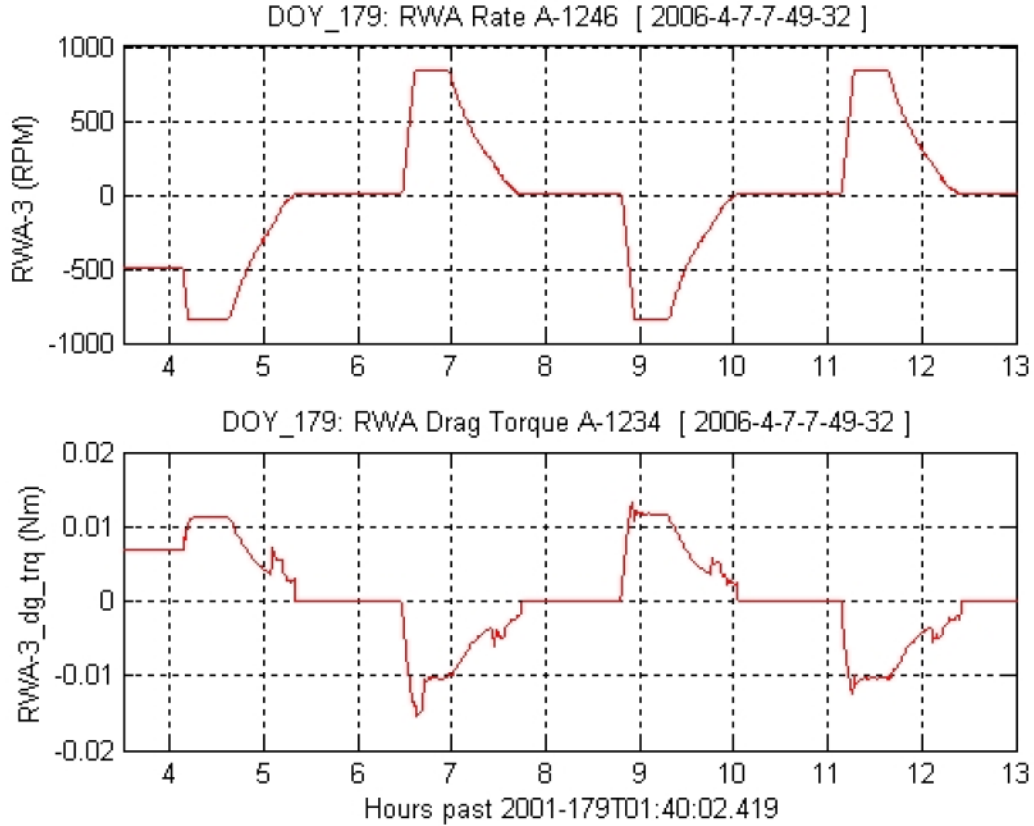


Figure 5. Telemetry of RWA-3 coast-down test performed in 2001

When a bearing ball comes into contact with the bearing race, the non-conformal contact between them will experience EHD lubrication. High pressures are generated in the contact zone, resulting in a significant increase in the viscosity of the lubricant. There are also significant deformations of the contacting surfaces. Both the increased viscosity of the lubricant and the elastic deformations of the contacting surfaces will assist in the formation of an effective lubricant film. To predict the film thickness, the EHD lubrication theory solves the classical Reynolds equation (the differential equation governing the pressure distribution in fluid film lubrication) in conjunction with the elastic deformation equations and the viscosity-pressure relation of the lubricant. In Refs. 8–9, the minimum lubrication film thickness (when normalized by the radius of the bearing ball) is found to be related to three dimensionless parameters: Speed parameter (U), Material parameter (M), and Load parameter (W).

$$\frac{h_{\min}}{R_E} \in f(M,W) \times U^p, \quad p = 0.68-0.73 \quad (5)$$

$$U = \frac{\eta \times R_p \times \omega}{E \times R_E}$$

In Eq. (5), $f(M,W)$ is a function of the dimensionless parameters M and W . Details on the definitions of M and W , and the function $f(M,W)$ itself are given in Refs. 8–9. The speed parameter U is defined in Eq. (5). The variable ω (rad/s) is the bearing spin rate, η (Ns/m²) is the nominal viscosity of the lubricant, E (N/m²) is the effective Young's modulus of the contact surface materials, R_E (m) is the effective radius of curvature of the two contacting surfaces, and R_p (m) is the pitch radius of the bearing. Accordingly to Eq. (5), the minimum lubricant film thickness (h_{\min}) grows with the spin rate according to ω^p ($p = 0.68-0.73$). The variation of the normalized minimum film thickness with the speed parameter U is depicted in Fig. 6. Obviously, low-rpm operation will lead to a small film thickness, and will increase the likelihood of metal-to-metal contacts between the balls and the races.

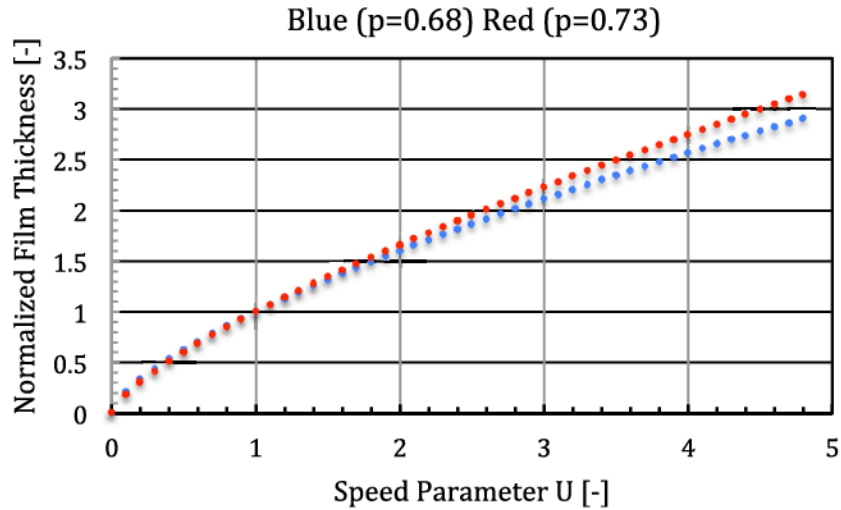


Figure 6. Variation of Lubricant Fluid Film Thickness with Bearing Spin Rate

The bearing spin rate that is required to achieve full EHD condition for the Cassini RWA bearings with the lubrication at 25 °C is estimated analytically to be 300–550 rpm. In Fig. 5, there was evidence that the bearings entered the boundary lubrication state at spin rates ≤ 250 rpm. The Cassini operation team selected 300 rpm as the EHD spin rate threshold to provide enough “room” between this rate threshold and the momentum limit of the reaction wheel (about 1,850 rpm, see also Section VI) to operate the wheels.

In Fig. 5, the spiky drag torque data observed below a spin rate of 250 rpm are obviously not consistent with Eq. (3). Hence, the RWAs’ viscous coefficients and Dahl drags are estimated using only spin rate data that are inside the range [+250, +836] rpm (or [-836, -250] rpm). Cassini mission operation team uses a nonlinear parameter optimization algorithm (which is based on the Nelder-Mead minimization methodology)¹⁰ to estimate the values of these parameters that best fit the time history the RWA spin rate $\omega(t)$.

Many coast-down tests performed after the year 2007 had experienced drag torque spikes of various kinds (see Section V). The resultant time histories of the RWA coast-down rates deviated significantly from the “smooth” spin rate profile exhibited in Fig. 5. An example is given in Fig. 7. This figure depicts the time histories of the estimated RWA-2 drag torque found during a ± 900 rpm coast-down test performed on 01/29/08. The counter-clockwise test was performed first and it generated good and useful data. The corresponding time history of the RWA spin rate was used to estimate the CCW drag parameters. The clockwise test was performed next and noisy data was found. Data found from the CW coast-down test could not be used to estimate the drag torque model parameters.

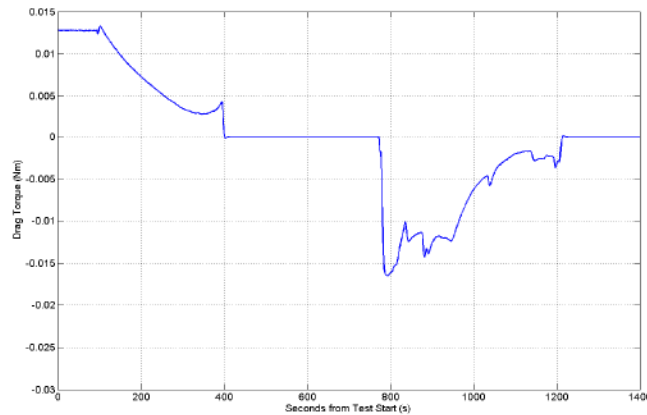


Figure 7. Estimated RWA-2 drag torque (coast-down test performed on 01/29/08)

The variations of the estimated mean bearing viscous coefficients of RWA-1 to RWA-4 over the year 2000–2009 are depicted in Fig. 8. Pre-launch, the mean viscous coefficients of RWA-1 to RWA-4 were estimated to be 11.4, 9.9, 9.9, and 9.9×10^{-5} Nms/rad, respectively. To better understand these trends, we note that the RWAs were first used to perform spacecraft attitude control on 16 March 2000, several months ahead of the Jupiter science campaign that began on 1 October 2000. Between March 2000 and December 2003, the wheels were used to maintain a quiescent spacecraft attitude during three long-duration gravitational wave experiments (26 November 2001 to 4 January 2002, 6 December 2002 to 14 January 2003, and 10–30 November 2003). Thereafter, use of the wheels became more intense beginning at the Approach science phase (January-June 2004) and at the start of the prime mission (July 2004). Also, one should note that, in the coast-down mode (with the D.C. motor powered off), the temperatures of the wheels were approximately 20 ± 3 °C.

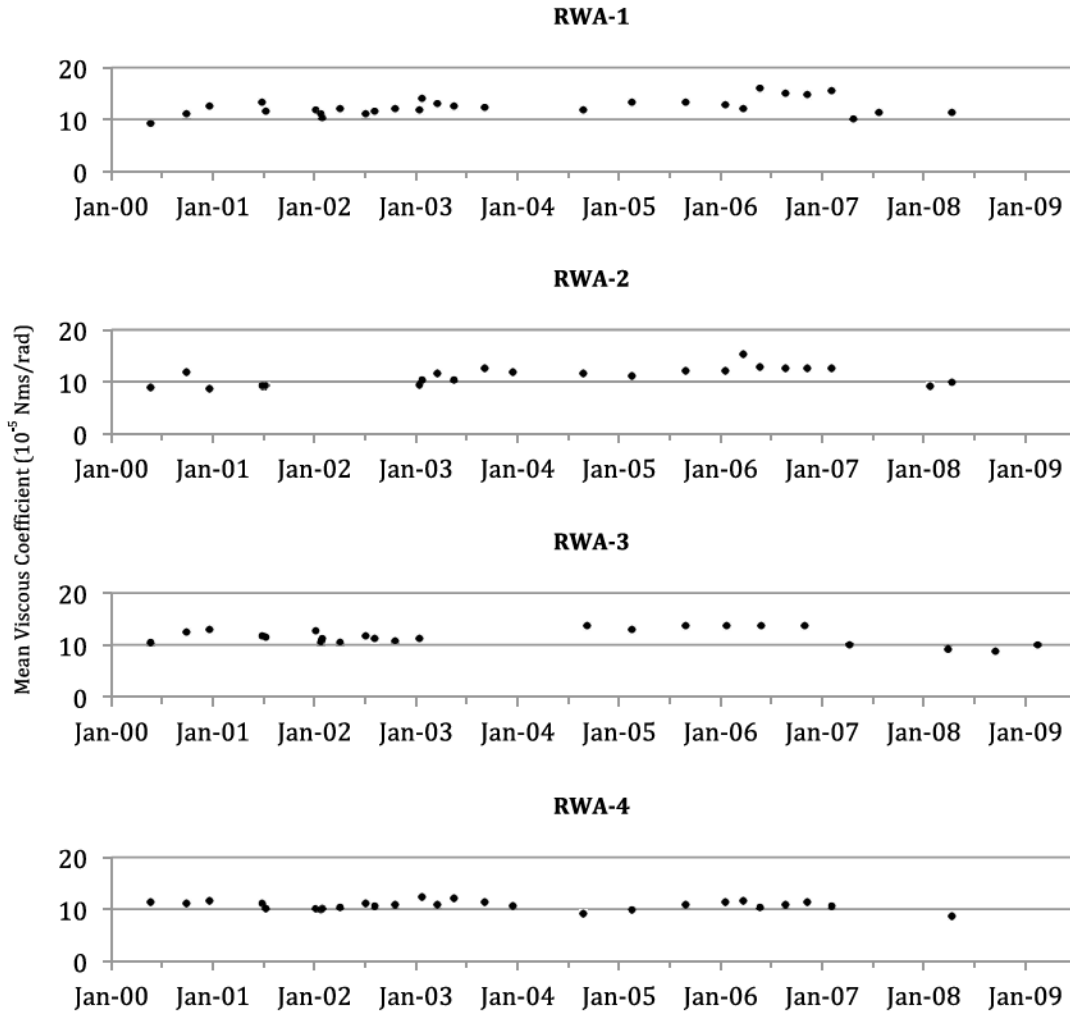


Figure 8. Trends of Cassini reaction wheel bearing viscous coefficients in 2000–2009 (Some test data are not usable)

In between March 2000 to December 2003, the viscous coefficients of RWA-1, 2, 3, and 4 were found to be higher than their respective pre-launch estimates by about 15–30%. In between January 2004 to December 2008, the viscous coefficients of RWA-1 and 2 were found to increase further to as high as 50–60% above their respective pre-launch estimates. However, in the same time period, the viscous coefficient of RWA-4 was only about 15–30% higher than its pre-launch estimate. This is likely due to the fact that RWA-4 was used for attitude control only beginning July 2003. In Section IV, details on an anomalous

RWA-3 bearing drag condition called cage instability will be described. The RWA-3 bearing drag torque anomaly was first observed in October 2002 and appeared/disappeared in the time period from October 2002 to June 2003. As indicated in Fig. 8, the occurrence of this drag anomaly wasn't preceded by any abnormal trend in the RWA-3 viscous coefficient. After the occurrences of these RWA-3 cage instability anomalies, most RWA-3 coast-down tests generated unusable data. This explains the "missing" RWA-3 viscous coefficient data from January 03 to July 04 in Fig. 8.

There were three coast-down tests performed in 2000 for the four wheels. The mean viscous coefficients of RWA-1 determined using data from these tests, in the clockwise and counter-clockwise directions, were $[11.0, 10.9] \times 10^{-5}$ Nms/rad, respectively. The mean [CW, CCW] viscous coefficients of RWA-2, RWA-3, and RWA-4 determined using data from the same set of tests, were $[9.3, 10.1] \times 10^{-5}$, $[12.3, 11.5] \times 10^{-5}$, and $[10.9, 11.8] \times 10^{-5}$ Nms/rad, respectively. Note that the mean CW viscous coefficients of all wheels were within 10% of their CCW counterparts. There were five coast-down tests performed in 2006 for the prime wheels (RWA-1, RWA-2, and RWA-4). The mean [CW, CCW] viscous coefficients of RWA-1 determined using data from these tests, were $[15.5, 12.8] \times 10^{-5}$ Nms/rad. For unknown reasons, the mean viscous coefficient in the clockwise direction was found to be about 20% higher than its CCW counterpart. The mean [CW, CCW] viscous coefficients of RWA-2 and RWA-4 were $[13.2, 13.0] \times 10^{-5}$ and $[11.0, 11.1] \times 10^{-5}$ Nms/rad, respectively. The mean CW and CCW viscous coefficients for RWA-2 and RWA-4 were nearly the same in 2006. Based on these observations, the Cassini operations team did not intentionally bias the RWA to operate them in either the clockwise or counter-clockwise direction.

The hydrazine cost of a RWA coast-down test depends on both the initial RWA spin rate of the test and the possible occurrences of drag spikes during the coast down of the wheels. The hydrazine cost of the ± 900 rpm RWA-124 coast-down test performed on 2004-DOY-243 was about 21 g. That for the ± 600 rpm RWA-34 coast-down test performed on 2004-DOY-256 was about 13 g. Using these representative hydrazine costs, the total hydrazine cost of performing all the RWA coast-down tests listed in Table 1 is about 1.3–1.4 kg. It wasn't low. As such, a decision was made in late 2009 to terminate these RWA coast-down tests in order to save hydrazine. Thereafter, the drag torque performance of the RWA bearings was monitored using only the telemetry of the estimated drag torque.

IV. Cassini RWA Bearing Cage Instability (CI)

Beginning 18 October 2002, the bearing(s) of RWA-3 developed a *bearing cage instability* condition that appeared (and disappeared) abruptly and unpredictably. A bearing cage is a rotor that rotates circumferentially with the bearing balls. As the bearing spins, the cage intermittently impacts one and then another bearing ball. At the contact interfaces (between the balls and the cage), a tractive force is developed that acts on both the balls and the cage, causing them to move (back and forth circumferentially, axially, and radially). Bearings are designed to withstand these "rubbings" via the use of balls made of hardened alloy steel. The magnitude of the tractive force depends on the lubrication at the critical interfaces. The magnitude of the tractive force and the coefficient of restitution between the cage and the balls (that controls the bouncing between them) decide whether the motion of cage will damp out or continue.¹¹ Without adequate lubrication, the tractive force will be large leading to uncontrolled vibration of the bearing cage that can cause intermittent and erratic torque transients, with accompanying loud noise (or squeal). The poor lubrication at the interfaces might be a result of lubricant starvation of the bearing, degraded lubricant's properties, migration of lubricant due to a thermal gradient from the hot contact surfaces (due to the repeated cage/ball "rubbings") to colder bearing regions, migration of lubricant due to a surface tension gradient from the hot contact surfaces to colder bearing regions (Gibbs-Marangoni effect, surface tension decreases with an increase of temperature), and/or bearing balls blocked or restricted lubricant flow to the critical cage/ball (and cage/race) interfaces.

The observed symptoms of bearing cage instability from Cassini flight telemetry data include:

1. An abrupt step-up of the bearing drag torque, followed by an abrupt step-down of the bearing drag torque at an unpredictable time later. In this paper, the magnitude of the drag torque increase is termed "*Drag torque step*". The duration the bearing is at the elevated drag torque condition is termed "*Duration*."
2. Superimposed on the elevated bearing drag torque are small drag torque oscillations. Half of the magnitude of the peak-to-peak variation of the drag oscillation is termed "*Roughness*." The (nearly constant) oscillation frequency is termed "*Frequency*".

These observed symptoms are consistent with those observed in the bearings of reaction wheels and control moment gyroscopes used by spacecraft.^{12,13} Fig. 9 depicts the time histories of the estimated RWA-3 drag torque from 2002-DOY-292T00:00:00 to 2002-DOY-294T00:00:00. Three occurrences of bearing cage instabilities were detected at the following times (times given represent the “start” time of the cage instability anomalies): 2002-DOY-292T09 (+382 rpm), 2002-DOY-293T06 (+382 rpm), and 2002-DOY-293T14 (-400 rpm). Note that all cage instabilities occurred at spin rates that were outside (but were very close) the sub-EHD region. The range of the *drag torque step* was 5–6 mNm. The *duration* of these cage instabilities was 4–9 hours. The *roughness* of the cage instability was 3 mNm, and the *frequency* of the drag torque oscillations was 8.8–10.6 mHz.

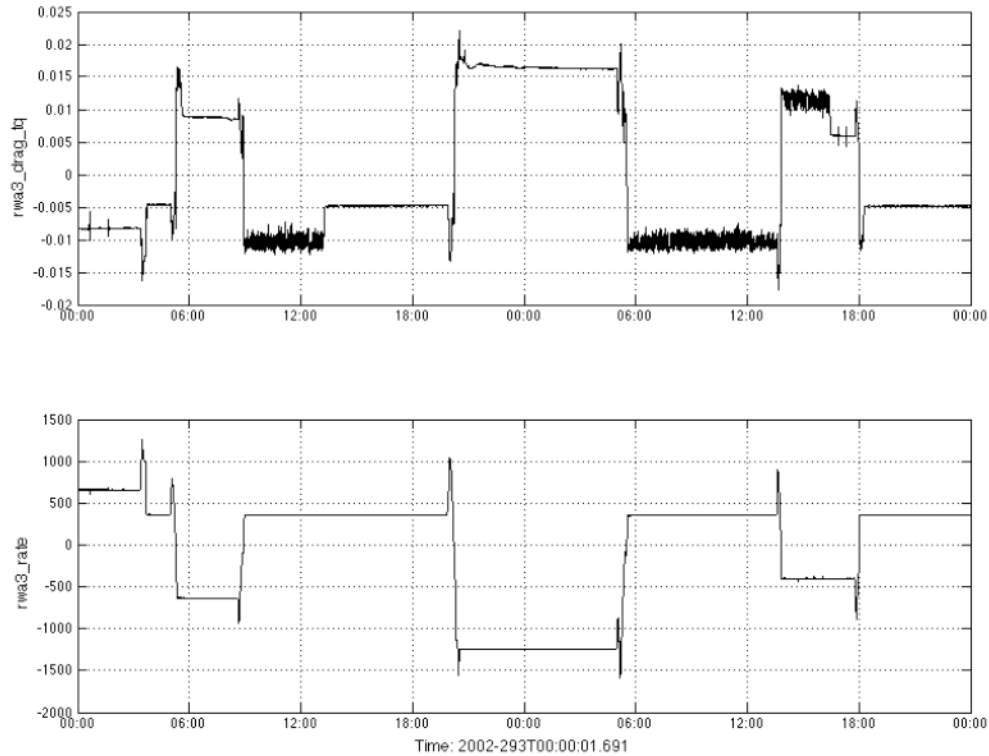


Figure 9. First three occurrences of RWA-3 bearing cage instability in 2002

Bearing cage instability is one of the most troublesome failure modes afflicting bearings due to the “come and go” nature of the anomaly. Bearing cage instability promotes energetic vibrations of the cage that lead to local heating of the cage as well as some bearing balls. In turn, the heating could cause polymerization of bearing lubricant (“gelled” oil). Ultimately, bearing cage instability can lead to premature bearing failure. Lubricant deprivation at the ball-cage interface has been shown to cause cage instability.^{11,14–15} The resultant high tractive force at the cage/ball interfaces triggers the vibratory motion of the cage. This is our conjecture on what caused the observed cage instability in the bearing(s) of RWA-3. Reaction wheels of several past spacecraft missions had failed due to persistent occurrences of this condition.¹³

The impacts of the anomalous RWA-3 drag conditions were greatly alleviated by the “drag torque estimator” function implemented in the RHM. As indicated in Fig. 3, the estimated bearing drag torque is added to the S/C attitude control torque and the total torque command is sent to the RWA D.C. motors. If the bearing drag torque is elevated, a larger motor torque command will be sent. As a result, the net impacts of the elevated RWA-3 drag torque on the S/C attitude control is being kept to a minimum.

After its first occurrence on 18 October 2002, the RWA-3 cage instability anomaly reappeared repeatedly and unpredictably over the next nine months. The magnitudes of the drag torque steps observed in these months were 5–8 mNm. The durations of these anomalies were 2–50 hours, and the total duration

of all CI durations is about 390 hr. The cage instability anomalies occurred when the RWA rates are inside either [+300 to +1000] rpm or [-1000 to -600] rpm. The drag torque oscillation frequencies were in the range of 8–11 mHz (cf. Tables 2 and 3). The observed CI frequency seems to be an invariant independent of the bearing spin rate. However, this frequency is suspiciously close to the bandwidth of the drag torque estimator (0.01 Hz, or 10 mHz). The actual vibratory frequency of the cage motion might have been significantly higher. However, the high-frequency motions were “low-pass” filtered by the 10-mHz PI drag torque estimator.

Table 2. A comparison of bearing cage instability symptoms observed in 2002–3 and 2011

Bearing CI drag characteristics	2002–3	2011
Drag torque step size [mNm]	5–8	3–9
Drag oscillation frequency [mHz]	8–11	3–9
Roughness [mNm]	2–3	0.5–2.5
Individual CI duration [hour]	2–50	1–96
Abundance [%]	8.7	19.7
Range of CW spin rate with CI [rpm]	300 to 1000	300 to 1500
Range of CCW spin rate with CI [rpm]	-1000 to -600	-1000 to -700

In spite of the drag torque compensation function performed by the RHM, the repeated occurrences of this anomalous bearing drag condition still threaten the long-term health of the wheel bearings. Because there is no sign that the cage instability condition will stop by itself, a decision was made to replace RWA-3 by the backup wheel (RWA-4). This change was successfully performed on 11 July 2003.¹ Thereafter RWA-3 was only used during the periodic drag torque characterization tests (see Table 1). However, two exceptions were made in November 2010 and March–April 2011 (details are given below).

Although the performance of the remaining three operational reaction wheels has been nominal, their identical bearing and lubricant design suggests that they too could be subject to the cage instability anomaly. Hence, in 2002–3, the Cassini project has taken the following steps to control reaction wheel performance degradation:

1. Kept RWA use to an absolute minimum during the outer solar cruise phase of the Cassini mission (2002–2004) to ensure RWA availability for science operations during the prime mission (from July 04 to July 08).
2. Uses a Cassini-developed ground software tool named Reaction Wheel Bias Optimization Tool (RBOT) to select an optimal set of RWA bias rates so that the total RWA dwell time inside the problematic low-rpm region can be minimized. Details on RBOT are given in Section VI.
3. Continues to monitor and trend the performance of the reaction wheels (including RWA-3, which now serves as the backup).

After an 89-month “rest” (from July 2003 to November 2010), the RWA-3 bearing drag performance was checked-out in a 50-hr mini-test conducted in November 2010. In this test, the spin rate of the RWA-3 was commanded to change from 0 to +1500 rpm, in increments of 100, 200, or 300 rpm. The RWA-3 spin rate dwelled at those incremental spin rate steps for twenty minutes each. Thereafter, the RWA-3 spin rate was commanded from +1,500 rpm to -1,500 rpm, again in increments of 100, 200, or 300 rpm each. Post-test, the drag torque performance of the wheel bearings was studied in details. No cage instability drag torque anomaly was observed.

Encouraged by the “nominal” performance of the RWA-3 in November 2010, RWA-3 was re-introduced as a prime wheel (together with RWA-1 and RWA-2) in the S67 science observation sequence. The sequence started on 7 March 2011 and lasted for about 45 days. Unfortunately, bearing cage instability symptoms reappeared in the drag torque telemetry of RWA-3. Two occurrences of the reappeared cage instability drag torque are depicted in Fig. 10. This particular anomaly was observed when the RWA-3 spin rate was maintained nearly constant at 1,000 rpm and +300 rpm.

Altogether, there were 18 distinct cage instability occurrences observed in the S67 science observation sequence. The total time duration that the RWA-3 bearings operated with the cage instability condition was about 210 hr. A comparison of the characteristics of cage instability symptoms observed in 2002–3 and 2011 is given in Table 2. Observed conditions that triggered CI appearances include the following:

1. Maintaining the RWA-3 spin rate at a constant rpm for a time duration that is >0.5 hr.

2. After a CCW to CW RWA-3 spin rate “zero crossing”.
3. After a CW to a CCW RWA-3’s spin rate “zero crossing”.
4. The RWA-3 spin rate was operated very close to the boundary of the sub-EHD region (+300 rpm).
5. The RWA-3 spin rate was operated close to the boundary of the sub-EHD region (-500 rpm).

In addition to RWA-3, another reaction wheel, RWA-2, also exhibited the CI symptoms but only for a brief time period. On 2009-DOY-260T03:14:00, RWA-2 spin rate was operating inside the rate range of [-1200 to -760] rpm, when its bearing experienced a drag torque “step” with signatures that were very similar to those observed in the bearings of RWA-3 (in 2002–03). Fig. 11 depicts the time history of the anomalous RWA-2 drag torque.

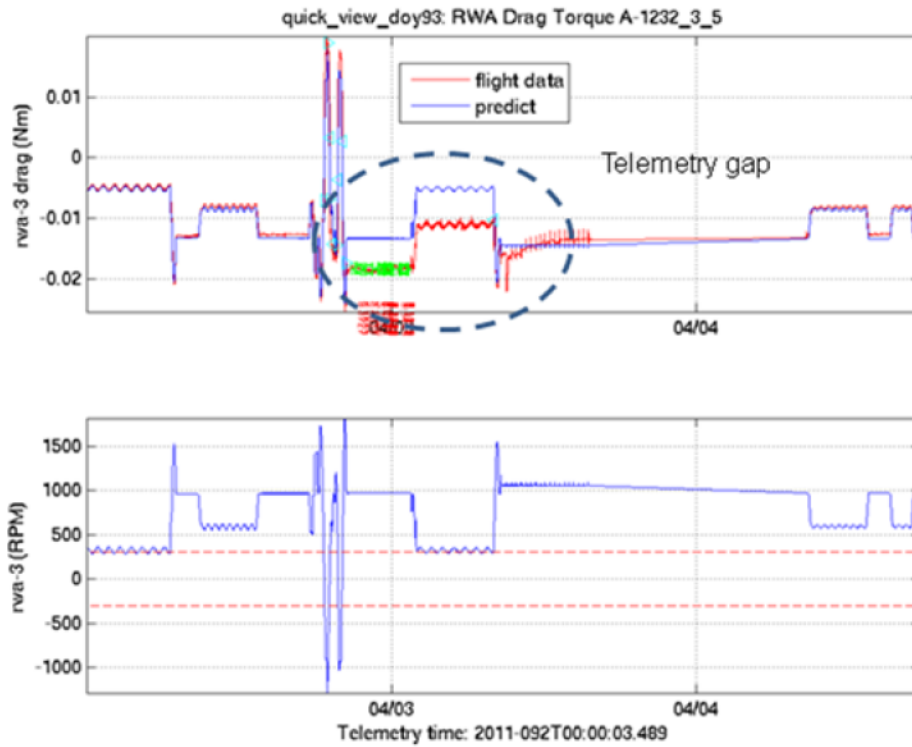
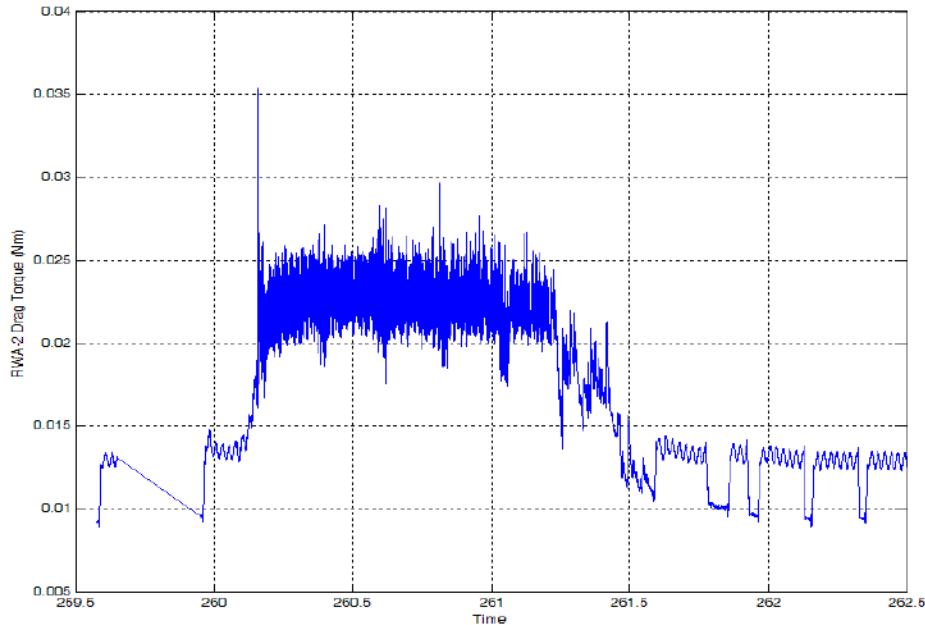


Figure 10. Reappearance of RWA-3 bearing cage instability anomaly in 2011



**Figure 11. RWA-2 bearing cage instability anomaly in 2009
(There is a data outage from DOY-259.7 to DOY-259.9)**

A comparison between the CI signatures of RWA-2 and RWA-3 cage instability anomalies is given in Table 3. After the brief CI occurrence in 2009, the RWA-2 bearing cage instability condition never reappeared. The bearings of RWA-1 and RWA-4 have never experienced any cage instability anomaly.

Table 3. A comparison of bearing CI symptoms in RWA-3 (2002–3) and RWA-2 (2009)

Bearing CI drag characteristics	RWA-3 (2002–3)	RWA-2 (2009)
Drag torque step size [mNm]	5–8	10
Drag oscillation frequency [mHz]	8–11	16
Roughness [mNm]	2–3	2.5
Individual CI duration [hour]	2–50	30

Dry bearing cage instability anomalies with symptoms very similar to those described above have also been observed in two (of four) attitude control reaction wheels of the ESA mission XMM-Newton.¹⁶ This X-ray Multi-mirror Mission (XMM) observatory was launched in 1999 for a 10-year mission. However, because both the spacecraft and its instruments are operating well, the mission has been extended to the end of December 2014 (potential future mission extensions are being considered). In 2011, the mission operation team detected cage instability in the bearing(s) of RWA-1. In reviewing RWA-1 engineering data since launch (in December 1999), they had discovered that those cage instability symptoms had actually been in telemetry data since 2008. A comparison of the Cassini’s wheel bearing CI symptoms and those of XMM-Newton is given in Table 4. In making this comparison, one must note that the cages of Cassini’s reaction wheel bearings are made of a crimped stainless steel ribbon whereas the cages of the XMM-Newton’s RWA bearings are made of a non-metallic cotton-based phenolic material. Also, each XMM-Newton’s wheel bearing is equipped with an oil-impregnated reservoir to provide lubrication for the lifetime of the wheel. However, in the time period of 1999–2011, no re-lubrication was ever performed on any wheel. The bearing(s) of a second XMM-Newton reaction wheel (RWA-2) has also experienced minor (<5% abundance) cage instability drag in 2011.

Table 4. A comparison of bearing cage instability symptoms in Cassini RWA-3 (2002–3) and XMM-Newton RWA-1 (2008-12)

Bearing CI drag characteristics	Cassini-Huygens RWA-3 (2002–3)	XMM-Newton RWA-1 (2008-12)
Drag torque step size [mNm]	5–8	18–20
Drag oscillation frequency [mHz]	8–11	Unknown
Roughness [mNm]	2–3	4–5
Abundance [%]	9-10	10–25
Individual CI duration [hour]	2–50	1–4
Range of CW spin rate with CI [rpm]	+300 to +1000	+600 to +3000
Range of CCW spin rate with CI [rpm]	-1000 to -600	-3000 to -800

V. Cassini RWA Drag Torque Spikes

Beside the class of bearing cage instability anomalies mentioned in Section IV, other anomalous drag torque signatures were also observed in all RWAs since the year 2000. The new class of anomalous drag torques is “spiky” in appearance, and the drag spikes usually occurred at time when the RWA was maintained at a constant spin rate. At a constant spin rate, the expected drag torque should be nearly constant. However, drag torque spikes were often observed superimposed on the “constant” drag torque. This initial impulsive rise in drag torque is often time followed by either a rapid (several minutes) or gradual (several hours) exponential decay to the nominal drag level. The spikes have a wide range of magnitudes and they occurred in a wide range of RWA spin rate conditions. Two sub-classes of anomalous drag torque spikes were observed and are described in the following.

The first class of anomalous drag torque spikes resembles the time history of the RHM’s response to an impulsive drag depicted in Fig. 4. After an abrupt onset of drag spike, the drag torque typically decayed to the nominal drag level in 6–7 min. This class of anomalous drag symptoms first occurred in November 2000. A representative drag spike is given in Fig. 12. This figure depicts the time history of the RWA-4 drag torque observed on 2004-DOY-041 when RWA-4 was maintained at an almost-constant rate of +271 rpm. With no obvious reason, several drag spike transients with magnitudes of 0.2–1.5 mNm were observed. Note that these spikes decayed to the nominal level quickly, in 6.5–7 min. This timing is longer than the settling time of the drag estimator (about 1.5 min., see Section II).

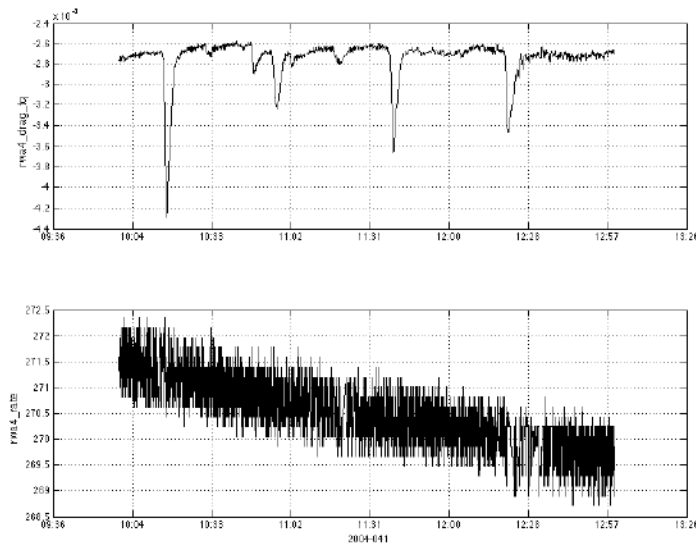


Figure 12. Spiky RWA-4 drag torque observed at a constant spin rate of +271 rpm on 2004-DOY-041

The second class of anomalous drag spikes is also “spiky” but it has significantly longer “settling” times. On 2006-DOY-266, a series of RWA-1 drag torque “spikes” was observed (cf. Fig. 13). RWA-1 was maintained at an almost-constant rate of -250 rpm when these anomalous drag spikes were observed. The magnitudes of these spikes were about 6–7 mNm. As depicted in this figure, the four observed drag spikes decayed to the nominal level slowly, in about 1.4–1.5 hrs (instead of several minutes). This particular series of drag torque spikes occurred almost immediately after spin rate reversals (or “zero-crossing”). There were many other instances when long-settling time drag spikes were observed after RWA spin rates’ zero crossing. Hence, speed reversal might be a possible cause of this class of anomalous drag symptoms.

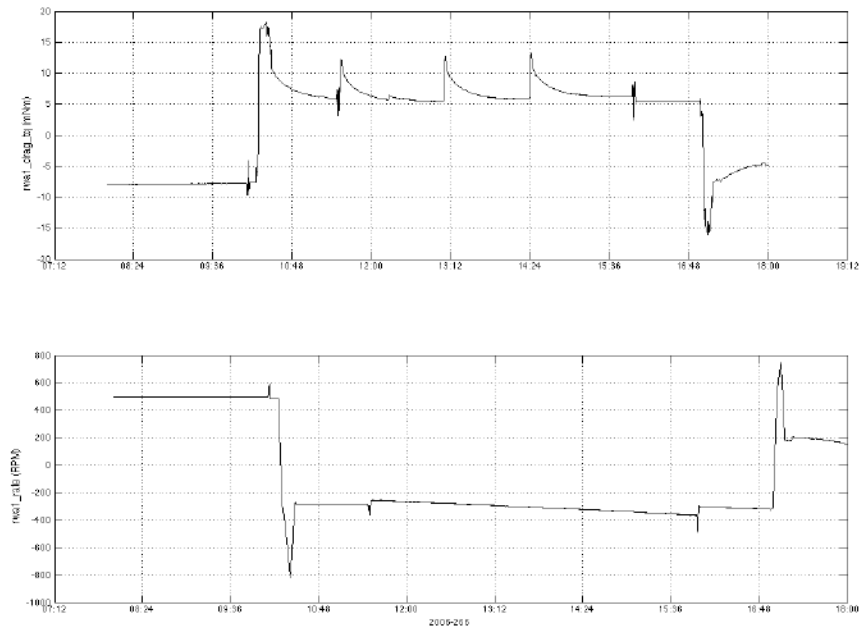


Figure 13. Spiky RWA-1 bearing drag torque spikes observed on 2006-DOY-266

The definite cause of these drag torque spikes is unknown. It is our conjecture that it is an “oil jog” phenomenon: a rapid incorporation of a small amount of lubricant by the bearings followed by its relatively slow dispersal. Bearings can have small pockets of lubricant that collect outside of the normal ball/cage and ball/race contact areas. They can become entrained in the contact areas by a variety of processes. Bearings that suddenly encounter an addition of oil will show an abrupt increase in drag that will then dissipate. The size of the drag torque spike and the time required to redistribute the oil depend on the amount of oil in question and the RWA spin rate at the time the spike occurred. If this conjecture is right, it is actually a positive indication of the presence of useful oil in bearings.

Relatively speaking, both RWA-1 and RWA-3 have the largest number of drag spikes, followed by RWA-2, and RWA-4 has the least number of drag spikes. For brevity, only the statistics of the RWA-1’s drag spikes are described in this paper. Figs. 14 and 15 depict the trends of the RWA-1 drag spike magnitude and “settling” time in 2000–2005, respectively. Note the presence of a large number of spikes during the Jupiter observation campaign (2001±3 months) and in the first 94 days of 2004 (the Approach science observation campaign). The wheels were used more extensively during these science observation campaigns. Hence, not surprisingly, more spikes were observed.

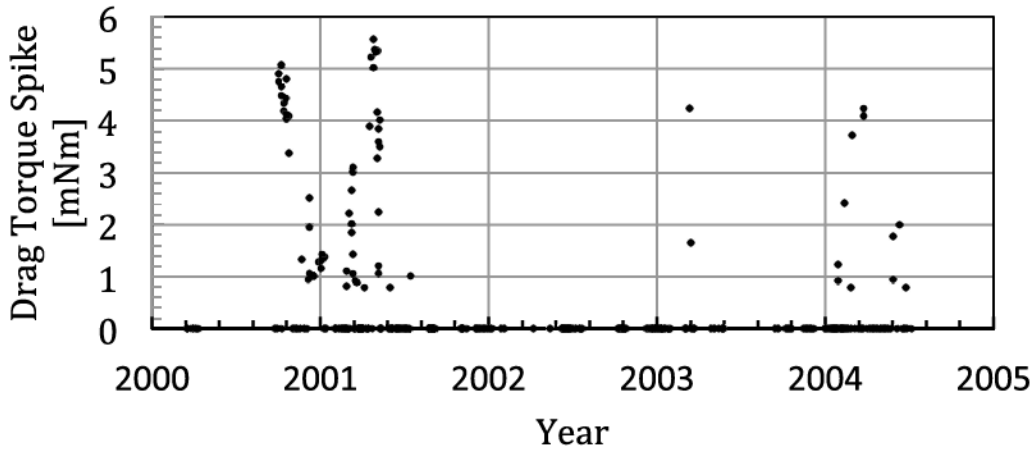


Figure 14. Trend of RWA-1 bearing drag spike sizes in 2000–05

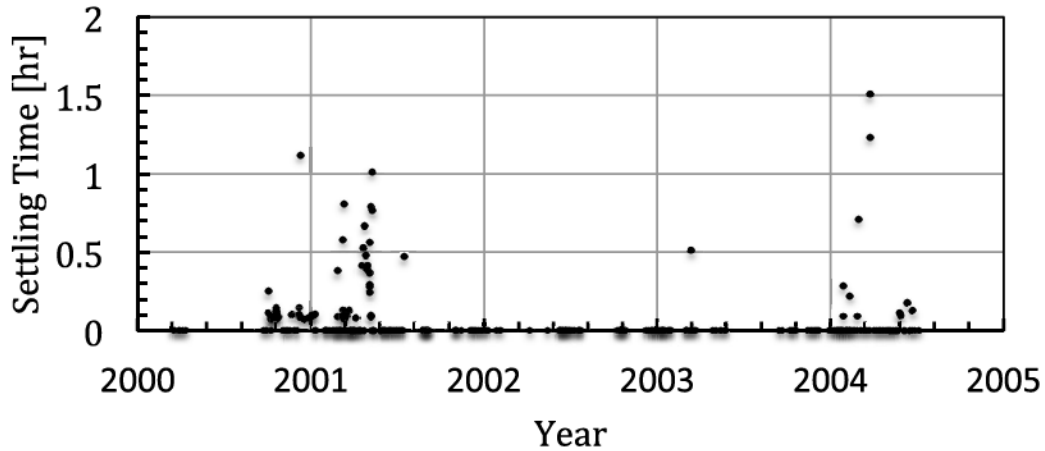


Figure 15. Trends of RWA-1 bearing drag spikes’ settling times in 2000–05

Fig. 16 depicts the trend of the RWA-1 drag spike magnitude in 2004–2007. Note that in mid-2004, there was a large RWA-1 drag torque spike whose magnitude was larger than 17 mNm. If the drag spike is small and is fully compensated by the drag torque compensation function of the RHM, it will not affect the S/C attitude control performance. However, large drag spikes could exceed the threshold of one of the RHM drag torque limiters (see Section II). When that happens, the partially compensated drag torque might impact S/C attitude control and trigger an error monitor (e.g., the RWA rate control error monitor), leading to a transition of control from reaction wheels to thrusters. To prevent the occurrence of such an unacceptable control mode transition (which has a significant hydrazine penalty), the thresholds of the torque limiters (of all the RWAs) were raised.⁴ To date, there has never been any accidental triggering of FP responses. The spin rates at which RWA-1 drag spikes occurred are also given in Fig. 16. Here we note that most drag torque spikes occurred while the bearings were operated within ± 900 rpm. In the years 2004–2007, it happened that RWA-1’s operated mostly in the CCW direction. Hence, most of the drag spikes occurred when RWA-1 operated in the CCW direction. Similar drag torque spikes were also observed in the telemetry of the other three wheels. Relatively speaking, RWA-1 bearings seem to have the largest and most frequent drag torque spikes in the year 2000–2007.

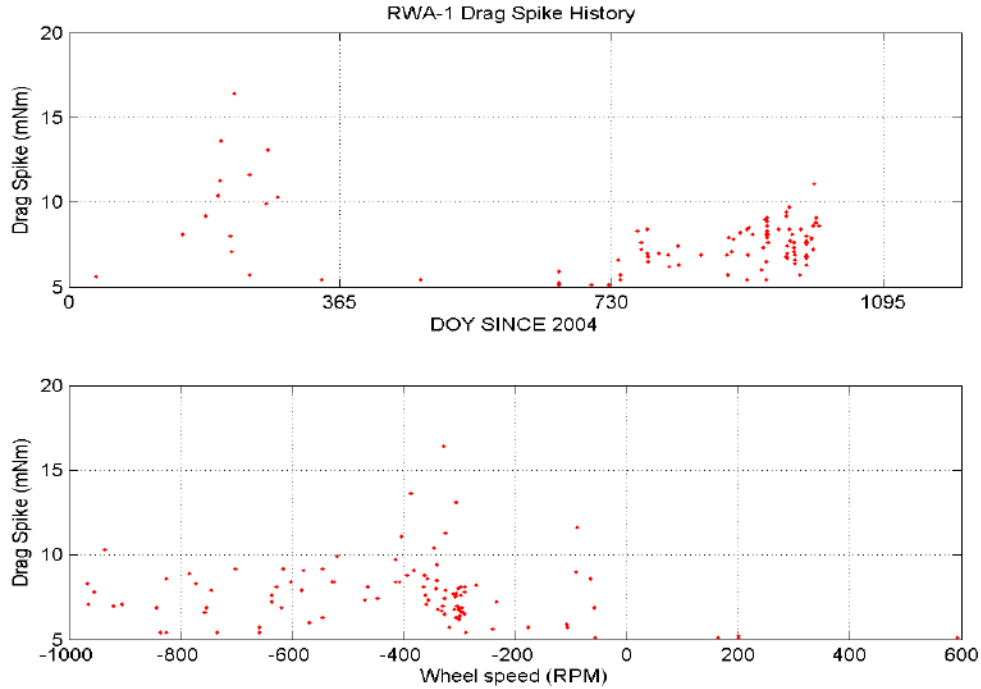


Figure 16. Trends of RWA-1 bearing drag spikes in 2004–07

VI. RWA Bias Optimization Tool¹⁷

In general, the use of reaction wheels for spacecraft attitude control is subjected to three constraints. First, at no time should any wheel rates be allowed to exceed the angular momentum capacity limit (about $\pm 2,020$ rpm) of the wheels. In fact, the on-board fault protection design will initiate an autonomous reaction-wheel-to-thruster control mode transition when an “Excessive RWA spin rate” condition is detected. Second, the total number of revolutions of the three prime wheels that is incurred as a result of science slews must be kept as low as possible. The requirement on the useful “life” of each reaction wheel is 4 billion revolutions.¹ These two constraints discourage high-speed wheel operations. Third, the operational hours the wheels spent inside a “low-rpm” region (assumed to be ± 300 rpm) must also be minimized. The requirement on the allowable sub-EHD dwell time of each wheel is 12,000 hours.¹ There is also an obvious need to ascertain that the three prime RWA will not draw power that exceeds the allocated power. For Cassini mission operations, power is never an issue.

The combination of these low-speed and high-speed RWA spin rate constraints can present a significant challenge to the Cassini operation team on the use of RWAs to support complex science slews over a long period of time. To protect Cassini against an accidental violation of any of these constraints, a ground software tool named Reaction Wheel Bias Optimization Tool (RBOT) was developed by the Cassini operations team for the management of the Cassini RWA.¹⁷ Given the time histories of the spacecraft’s attitude and attitude rate commands (to meet science observation needs), from the start to the end of a RWA biasing time segment, RBOT will select a set of optimal biasing rates for the three prime RWA that minimizes a cost functional J . In a simplified form, the cost functional J is defined as follows:

$$\text{Min}_{\omega_{RWA}} J = \sum_{i=\text{Prime RWA}} W_i \left\{ \int_{t=\text{Bias Start}}^{t=\text{Bias End}} G(|\omega_i(t)|) dt \right\} \quad (6)$$

Here, $|\omega_i(t)|$ (i = three prime RWAs) denote the time histories of the magnitudes of the spin rates of the prime RWA’s. The relative importance of the three prime wheels is specified by the weights W_i . Given the time histories of the spacecraft’s per-axis slew attitude and attitude rate commands, estimates of the inertia properties of the spacecraft and the reaction wheels, and an estimate of the environment torque vector, the reaction wheel rates $\omega_i(t)$ (i = three prime wheels), from the start to the end of a RWA biasing segment,

could be computed via the principle of conservation of the total angular momentum vector of the spacecraft in an inertial reference frame. The “gain” $G(|\omega_i|)$ is a function of the magnitudes of the RWA spin rate ω_i . This function is designed to enforce the three operational constraints described above. The gain is large when the RWA spin rate falls inside a sub-EHD spin rate (e.g., ± 300 rpm) and it becomes very large when the wheel is nearly stationary. The gain is also very large if the spin rate exceeds a high spin rate threshold (e.g., 1,850 rpm). This will strongly “discourage” the RWAs from operating with spin rates that are too close to its momentum storage capacity of RWAs (e.g., $\approx 2,020$ rpm). The margin between 1,850 and 2,020 rpm is used to guard against RWA spin rate prediction error (made by RBOT) due to our inexact knowledge of the environmental torques, S/C and RWA inertia properties, and other factors. In between the high and the low rate limits (1,850 and 300 rpm, respectively), G has smaller value that increases linearly with the magnitude of the wheel spin rate. This will minimize the accumulation of RWAs’ angular revolutions. The RBOT software allows the users to make changes to any of the set of key system parameters (e.g., 300 rpm, 1,850 rpm, environmental torques, etc.). A graphical illustration of the gain function is given in Fig. 17.

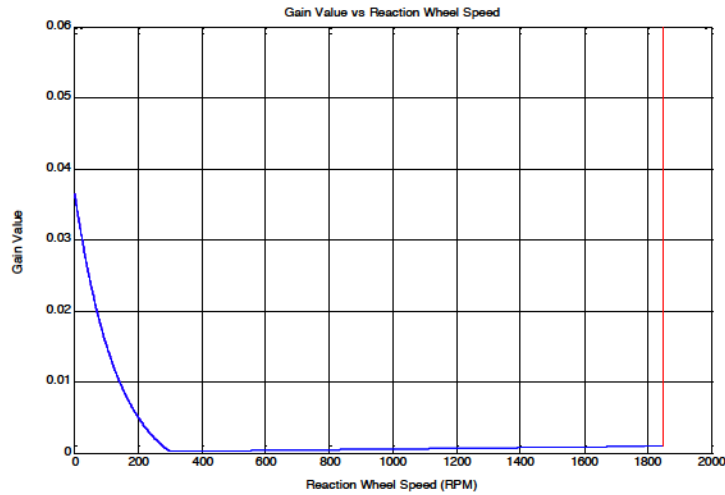


Figure 17. Gain as a function of the wheel speed used by RBOT¹⁷

The formulated nonlinear optimization problem is solved numerically using the Nelder-Mead simplex method.¹⁰ For each RWA biasing segment, RBOT will output multiple sets of candidate RWA biasing rates (for the three prime RWAs), in order of increasing cost functional J . Typically, the best set of RWA rates (with the smallest J) is selected. However, at times, a RWA bias rate set with a larger cost functional might be adopted. The effectiveness of RBOT is illustrated using the RWA biasing segment that spans 2004-DOY-212.5 to 2004-DOY-226.3. The time histories of the RWA spin rates are depicted in Fig. 18. Note that all the wheels spent very short time inside the sub-EHD region (± 300 rpm), and at no time do they get close to the $\pm 1,850$ rpm limit.

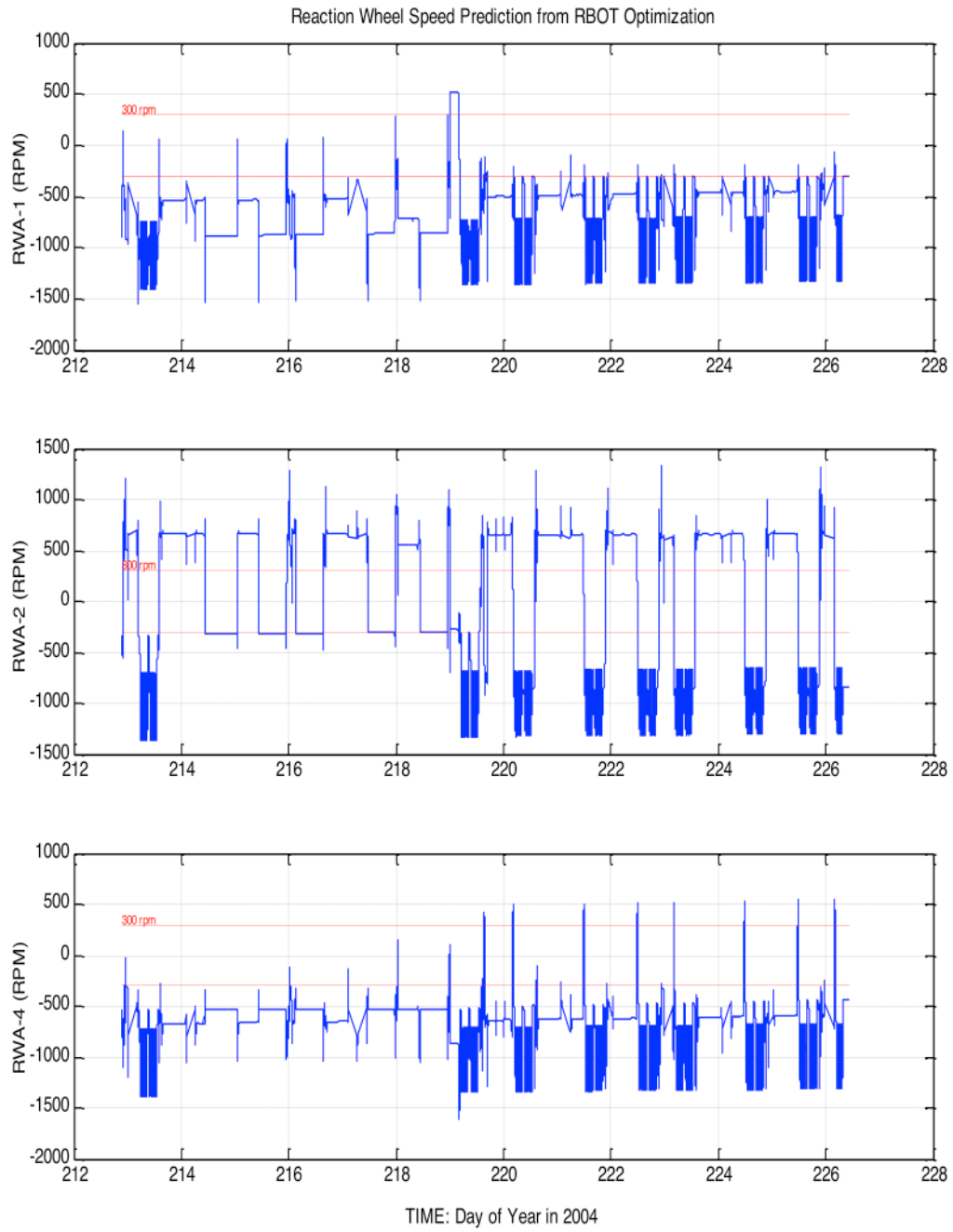


Figure 18. Reaction wheel speed prediction from an optimal RBOT bias solution

For some biasing segments with very complex science observations, it is possible that even the best set of RWA bias rates might still contain prolonged periods of spin rate dwelling inside the sub-EHD region. An example is given in Fig. 19. Note that in this particular RBOT solution, RWA-1 spin rate still spent 4.8 hours inside the ± 400 -rpm sub-EHD region (from DOY-217.7 to DOY-217.9). Also, RWA-4 spent another 4.8 hours inside the ± 400 -rpm sub-EHD region (from DOY-217.5 to DOY-217.7). This set of “best” RWA bias rates should not be blindly accepted. Instead, one or more of the following remedial actions should be aggressively pursued in order to protect the wheels:

1. Break the problematic biasing segment into two or more shorter biasing segments (but this will lead to a hydrazine penalty).
2. Modify some problematic science observation sequence designs (e.g., slew the S/C using slower rate and/or acceleration profile limits) to allow RBOT to find solutions without long dwelling inside the sub-EHD region.
3. Cancel some science observation sequences.

Other operations guidelines the attitude control team levied on the science teams that are used to better protect the reaction wheels are described in Ref. 18. Disciplined and long-term use of RBOT has led to a significant reduction in the daily consumption rate of the RWA low-rpm dwell time.

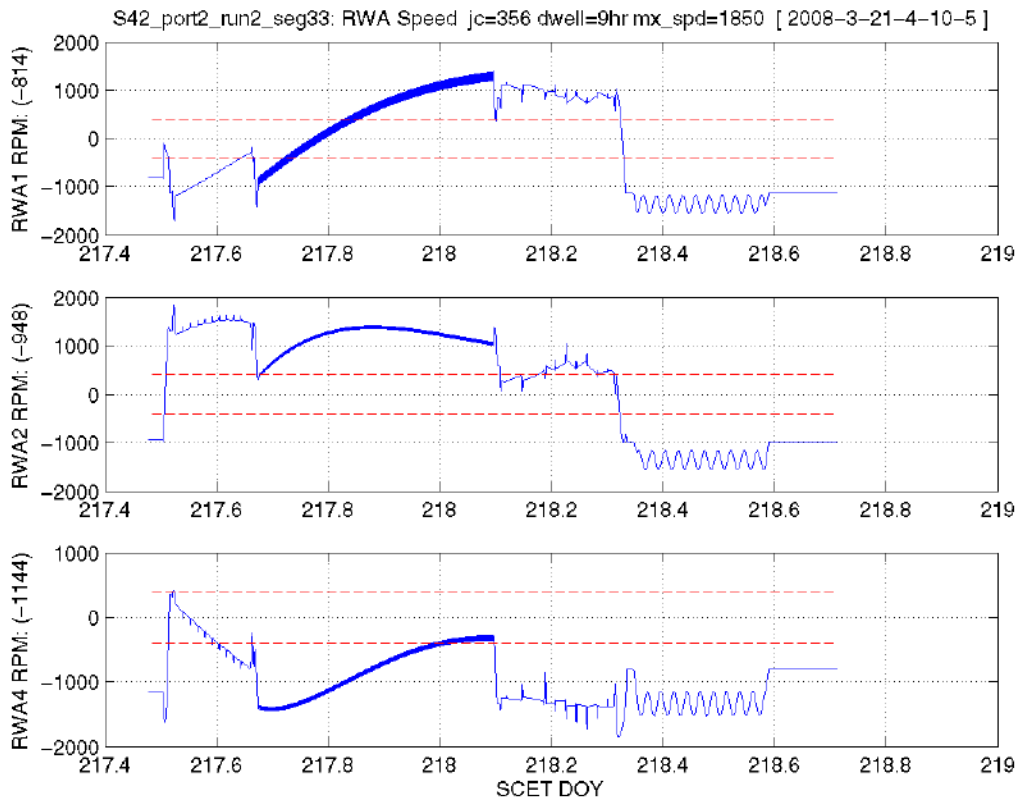


Figure 19. Both RWA-1 and RWA-4 spent 4.8 hours in the sub-EHD region in this “optimal” RBOT solution

VII. Statistics of RWA Consumables

The time variations of reaction wheels' revolutions in the year 1997–2013 are depicted in Fig. 20. The consumption rates of the three prime wheels, RWA-1, 2, and 4, in 2004–2013, are nearly the same, they are about 1.14 million revolutions per day (each). These consumptions have remained nearly constant since the start of the prime mission (July 2004).

The time variations of reaction wheels' low-rpm (± 300 rpm) times in the year 2003–2013 are depicted in Fig. 21. The consumption rates of the three prime wheels' low-rpm times are time varying and are decreasing with time. In 2005–06, the consumption rates were about 2.5 hours per day. In 2010–2013, the consumption rates are about 21 minutes per day. This drop in the time spent inside the ± 300 rpm sub-EHD region is due mainly to the disciplined use of the ground software tool RBOT.

The rate of RWA power on/off cycle for the three prime wheels (RWA-1, 2, and 4) are about 32 cycles per year (each).

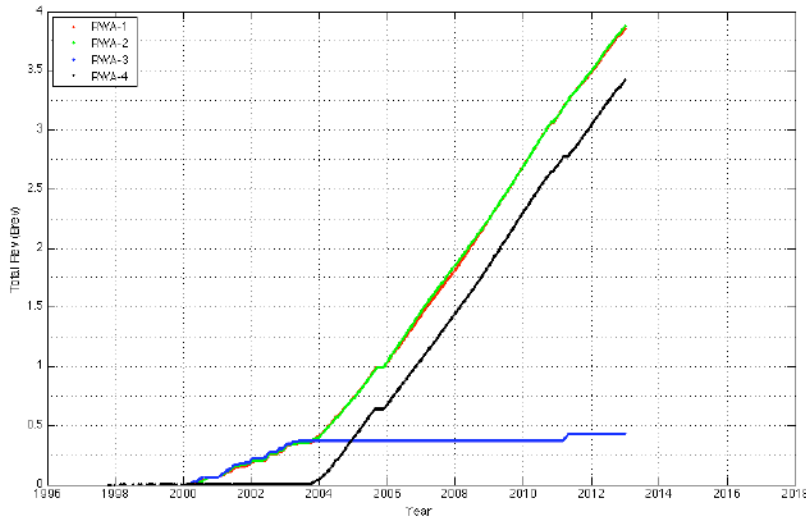


Figure 20. Trends of reaction wheels' revolutions in 1997–2013

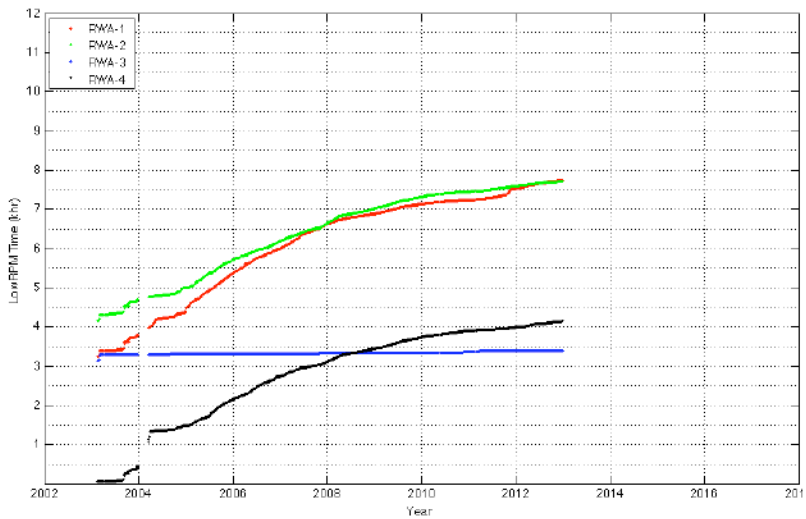


Figure 21. Trends of reaction wheels' low-rpm (± 300 rpm) time in 2003–2013

VIII. Cassini Candidate Hybrid Controller Designs

Hybrid controllers with mixed actuators had been designed and implemented on spacecraft with only two working reaction wheels. After two wheel failures, the Far Ultraviolet Spectroscopic Explorer (FUSE) restored its three-axis attitude control functionality using a hybrid controller with magnetic torque bars and two reaction wheels.¹⁹ A similar hybrid controller was implemented on the TIMED spacecraft.²⁰ After two wheel failures in 2004–05, the spacecraft Hayabusa (Muses-C) switched to a hybrid control configuration that used only one wheel and RCS thrusters.²¹ Hybrid controllers using two reaction wheels and attitude control thrusters have also been uploaded to the solar-electric propelled spacecraft Dawn.²² The wheels of FUSE, TIMED, Hayabusa, and DAWN all failed/degraded due to bearing problems.

To date, Cassini reaction wheels have accumulated more than 4 billion revolutions each (see Section VII). As such, in spite of careful management of the wheel spin rates by the mission operation team, there are observed increases in the drag torque of the wheels' bearings. To prepare for a contingency scenario in which RWA-1, in addition to RWA-3, has degraded to a non-working state, two candidate hybrid controllers have been designed and tested on the ground.²³ These candidate hybrid controllers each use two wheels and four thrusters, and are designed to meet the pointing needs of two key Cassini science modes: Optical Remote Sensing (ORS) and the Downlink, Fields, Particles, and Wave (DFPW) modes.

To meet the science needs of twelve science instruments, the Cassini mission operations team divides the 24-hour cycle into two distinct operation segments: 15 hours in the ORS mode and 9 hours in the DFPW mode. In the ORS mode, the spacecraft is slewed using the RWA's in order to point the optical bore-sight vectors of four remote sensing instruments (for example, the Narrow Angle Camera, NAC) to the inertial targets of interest. The inertial pointing control requirement for science observations made using these remote-sensing instruments is 2 mrad (X and Z-axis, radial 99%).¹ At the same time, the pointing stability of the spacecraft must meet requirements specified in Refs. 1–3.

In the DFPW mode, the High Gain Antenna (HGA) axis (which is aligned with the S/C's Z-axis) is pointed at Earth with an inertial pointing control requirement of 3.14 mrad (X and Y-axis, radial 99%).¹ With this HGA-to-Earth attitude, ground-based commands could be sent to the spacecraft while telemetry data are transmitted to the ground from the spacecraft. At the same time, without changing the HGA-to-Earth attitude, the spacecraft is commanded to spin about the Z-axis at the commanded spin rate. A representative spacecraft spin rate is 3.1 mrad/s. With a spin rate, the six Fields, Particles, and Plasma Waves instruments could collect science data as they scan the 360° sky.

In the ORS mode, both the pointing control and pointing stability requirements about the spacecraft's X and Z-axis are stringent. Hence, it made sense to use the two working reaction wheels to perform attitude control about these two axes while the Y-axis is controlled via four thrusters. In the DFPW mode, the HGA pointing control requirement about the spacecraft's X and Y-axis is stringent. Hence, it made sense to use the two reaction wheels to perform attitude control about these two axes while the Z-axis is controlled using thruster couples. Details associated with both the ORS and DFPW hybrid controllers are given in Ref. 23.

Simulation results of a representative ORS science observation mosaic scenario indicated that the performance of the ORS hybrid controller is good when compared with an all-thruster control system.²³ In Table 5, a comparison of the performance of these alternative control configurations is made. Note that the ORS hybrid controller can achieve attitude and attitude rate control errors that are an order of magnitude better than their counterparts achieved using an all-thruster control system. Also, the hydrazine consumption rate of the hybrid controller is about 3.5 times smaller than that of an all-thruster control system. However, large angle spacecraft slews about either the X or Z-axis made using the ORS hybrid controller will saturate the reaction wheels. An alternative hybrid controller is needed for the DFPW scenario.

The DFPW hybrid controller could achieve excellent attitude control performance of the S/C's X and Y-axis, meeting the stringent pointing control requirement of the HGA. However, any attempt to control the S/C's Z-axis spin rate using the Y-facing thrusters will incur heavy hydrazine penalty (due mainly to the need to overcome gyroscopic torque generated by slewing a S/C with two spinning RWAs). One way to work around this limitation is to first spin-up the S/C using the Y-facing thrusters to a nominal S/C's Z-axis spin rate. Thereafter, control about the S/C's Z-axis is *disabled*, and the spacecraft's Z-axis rate is allowed to fluctuate freely according to the conservation of the total angular momentum of the S/C (in an inertial frame). However, in this "no Z-axis control" control configuration, the spin rates of both reaction wheels will fluctuate about zero-rpm, leading to multiple speed reversals (zero-crossings) of the wheels' bearings.

At the same time, the wheels' rpm will dwell within the EHD speed limits (± 300 rpm) for significant ($\approx 19\%$) time duration. Both conditions are known to cause accelerated degradation of the wheel bearings. In Table 6, the performance of the all-thruster controller is compared with that of the DFPW hybrid controller.

Table 5. Figures of Merit: ORS Hybrid Controller vs. All-thruster Controller

Figures of Merit	Units	ORS Hybrid Controller	All-thruster Controller [†]
Peak attitude control error:			
X-axis	mrads	± 0.07	± 2.0
Z-axis	mrads	± 0.10	± 2.0
Peak instantaneous line-of-sight rate:			
X-axis	mrad/s	± 0.011	± 0.19
Z-axis	mrad/s	± 0.020	± 0.14
Hydrazine consumption rate	gram/hr	10.6	36.9
Total ΔV magnitude generated at end of mosaic (Y-axis dead-band = 2 mrads)	mm/s	3.15	11.3

[†]With per-axis attitude controller dead-band of [2,2,2] mrads.

Table 6. Figures of Merit: DFPW Hybrid Controller vs. All-thruster Controller

Figures of Merit	Units	DFPW Hybrid Controller	All-thruster Controller ^a
Peak attitude control error:			
X-axis	mrads	± 0.01	± 2.0
Y-axis	mrads	± 0.01	± 2.0
Peak instantaneous rate:			
X-axis	mrad/s	± 0.0015	± 0.05
Y-axis	mrad/s	± 0.0015	± 0.05
Z-axis spin rate	mrad/s	$3.07 + \Delta\Omega^b$	3.07 ± 0.05
Time to complete 10 revolutions	Hour	5.1861	5.6851
Total hydrazine Consumption	gram	9.92^c	34.2
Total ΔV magnitude imparted at S/C	mm/s	0^d	20.63

^aWith per-axis attitude control dead-band of [2,2,20] mrads. See Ref. 23 for details.

^b $\Delta\Omega[\max] = +5.92$ mrad/s, and $\Delta\Omega[\min] = -1.81$ mrad/s.

^cSpin-up and spin-down of S/C to/from 3.07 mrad/s ≈ 9.92 grams. See Ref. 23 for details.

^dSpin-up and spin-down are performed via thruster couples. Net ΔV imparted on the S/C is nearly zero.

To implement these hybrid controllers, both the reaction wheel and thruster controller modules in the Cassini flight software would need substantial logic changes. Other supporting software modules such as fault protection, commands and telemetry, etc. must also be modified. The revised flight software must then be regression tested. The effort involved will be significant and work on the hybrid controllers should not be initiated lightly. However, if an unambiguous bearing degradation trend is observed in a second Cassini RWA (in addition to the degraded RWA-3), it is important to get ready with the implementation planning of these contingency hybrid controllers. Results documented in Ref. 23 revealed that with modifications to both the Cassini flight software and mission planning software, the hybrid controllers will allow for a continuation of the Cassini extended mission even with two degraded reaction wheels. The new control scheme will allow less flexibility in science observation scheduling than was enjoyed prior to wheel

failures, but three key science operation modes (ORS, DFPW, and Radio science) could still be at least partially supported. Demerits of these hybrid controllers have also been identified in Ref. 23.

IX. Recommended Practices for Management of Spacecraft Reaction Wheels and Conclusions

Many spacecraft with attitude controlled by reaction wheels (or control moment gyroscopes) had encountered bearing-related flight anomalies. Examples mentioned above include DSP, FUSE, Hayabusa, TIMED, Dawn, and XMM-Newton. More recently, the spacecraft Mars Odyssey, Kepler, and the ESA Rosetta have also experienced bearing-related anomalies. Over the past fifteen years (1997–2012), in “flying” the Cassini spacecraft, the Cassini mission control team has acquired some useful flight experience on good compromises between the science observation needs and the health and safety of the reaction wheels. Flight lessons learned are listed below (in random order).

1. Track RWA performance, beginning with wheel acceptance tests and throughout mission operations, to identify potential limitations on reaction wheel lifespan. Routine coast-down tests of all reaction wheels (both prime and backup) could generate data that allow mission operation team to monitor the health state of the wheel bearings. However, these coast-down tests must be designed in a way that minimizes both the thrusters’ fuel cost and the ΔV imparted on the spacecraft (which can complicate navigation).
2. Implement a reaction wheel drag torque estimator in the flight software to provide ground visibility of any anomalous bearing drag conditions such as cage instability. Mitigate the impacts of these anomalous drag torques on the overall spacecraft attitude pointing performance by a drag torque compensation system. The high-water marks of these drag estimates (of all wheels) should be trended to detect any worrisome trends.
3. To assist in minimizing the time the wheels spent within the sub-EHD region, use a ground software tool (e.g., RBOT) to carefully manage reaction wheel biasing events. This ground software tool should be continuously updated with the changing spacecraft’s inertia properties, environmental torques, relative health state of the wheels, and other factors. Attention must be given to feedback from the users of this GSW tool. The tool must be improved using these “voices of the customers.”
4. Aggressively and constantly look out for opportunities in science observation sequence designs that can reduce low-rpm RWA operations. Techniques include the addition of un-scheduled RWA biasing events, selections of alternative secondary vector pointing pairs in different segments of a RWA biasing window, and the use of different science slew rate/acceleration profile limits.¹⁸
5. Besides the spin rates of the reaction wheels, probably the next most influential parameter that controls the performance of the bearing lubrication system is the bearing temperature. Bearing temperature affects both the viscosity and the surface tension of the lubricant. Loss of oil through vaporization, creep, and chemical degradation of lubricant are also related to oil temperature. Therefore it is important for the operations team to ascertain that all the wheels’ bearings are being maintained within the acceptable temperature ranges of the powered-on (or off) wheels in all operating modes of the wheels (e.g., during coast-down tests when the D.C. motor torque has been removed as well as when the wheels are being used to control the spacecraft’s attitude). The acceptable operating temperature ranges of the Cassini reaction wheel mechanism in both the powered on and off states are given in Ref. 1. Throughout the past 15 years, the Cassini wheels’ temperatures have stayed within these ranges with margins.
6. Where RWA performance data indicates that the RWA lifespan may be constrained, take measures to mitigate the mission impact. For example, control the spacecraft’s attitude using thrusters before the start of the prime mission and for observations with pointing stability requirements that could be easily achieved using thrusters. However, attention must be paid to the resultant impacts on the budgets of hydrazine and the thrusters’ on/off cycles. Any identified “degraded” RWA should be “saved” for end-of-mission when most prime science objectives have already been successfully achieved.
7. Review the onboard fault protection design to identify its vulnerability when wheel drag torque is elevated. Should the thresholds and/or persistence limits of certain error monitors be changed? Should the FP response logic be modified? A Cassini flight experience is given here. Elevated wheel drag torque will trigger error monitors (e.g., the “excessive RWA rate control error”). The resultant FP response used to be only a wheel-to-thruster control mode transition, without calling “Safing”. Hence,

without being terminated by Safing, the onboard science observation sequences will continue on thrusters with serious hydrazine cost and ΔV implications. That design was subsequently modified: A Safing call is added to the FP response logic in order to terminate the onboard science observation sequence. In the end condition, the S/C maintains a quiescent Earth-pointed attitude, using thrusters, and wait for ground support.

8. Design, test, and exercise contingency procedures that will be needed to recover the S/C from a Safing state that is caused by a degraded/failed RWA. A contingency procedure that defines the steps necessary to return the spacecraft from the thruster-based Safing state to a wheel-based attitude control mode must be thought out in advance. This “master” contingency procedure might have to be supported by other contingency procedures such as:
 - a. The new reaction wheel control configuration might involve using the articulation reaction wheel in a position other than its current position. A procedure must be readied to perform the needed articulation motion.
 - b. Another procedure will be needed to determine the post-articulation position of the articulation wheel. One way to do that was described in Ref. 1.
 - c. Yet one more procedure will be needed to upload a set of commands with the estimated articulation wheel position to the flight software.
9. If unambiguous bearing degradation trends are observed in multiple reaction wheels well before the end of the prime (or extended) mission, it is important to get ready with the implementation planning of a contingency hybrid controller. Beside the design and testing of hybrid controller(s), preparatory work must also include the following:
 - a. Modifications of the existing test bed that could be used to characterize the performance of the hybrid controller (e.g., hydrazine consumption rate).
 - b. Identifications of new operational constraints that must be enforced via additional flight rules. For example, it might be more fuel-efficient to slew the spacecraft in two steps, one slew about an axis that lies in the plane of the two reaction wheels, and the second about an axis that is perpendicular to that plane.
 - c. Use of new values for design parameters of fault protection error monitors (e.g., thresholds and/or persistence limits of RWA-related error monitors).
 - d. Plan and execute an inflight checkout activity of the hybrid controller well before the hybrid controller is needed for prime mission science activity. Lessons learned from this checkout must be addressed.

Cassini carries multiple high-resolution scientific instruments for which proper operation demands a high level of spacecraft pointing stability. Comprehensive analyses to assess Cassini in-flight pointing-stability performance over the past years have been made³ and they indicated that all the pointing stability requirements are met with very significant margins. The foundation of this achievement is a set of “healthy” reaction wheels. Inflight performance of Cassini wheel bearing drag in 1997–2012 is summarized in this paper. Facing these anomalous drag torque symptoms, the Cassini mission operations team developed and used a ground software tool RBOT to manage the Cassini reaction wheel rates. Flight experience on the use of this ground software tool as well as other lessons learned on the management of Cassini reaction wheels are given in this paper. Many of the lessons learned by the Cassini mission operation team are equally applicable to future missions if attaining high pointing stability performance (by the wheels) is critical to mission success.

Acknowledgements

The work described in this paper was carried out by Jet Propulsion Laboratory, California Institute of Technology, under a contract with the National Aeronautics and Space Administration. Our colleague, Cliff C. Lee contributed to many analyses of RWA drag torque telemetry as well as the development of the ground software tool RBOT. We also want to thank T. Brown, T. Burk, E. Konefat, G. Macala, Dr. E. Maize, P. Meakin, Dr. R. Rasmussen, J. Savino, B. Smith, R. Weitzl, and J. L. Webster for their invaluable support. Discussions we made with both Drs. Stephen V. Didziulis and Peter P. Frantz of The Aerospace Corporation have helped us to better understand the tribology of the Cassini reaction wheels’ bearing lubrication system. We also wish to thank both Glenn A. Macala and Sima S. Lisman for their valuable reviews of earlier versions of this paper.

References

1. Lee, A.Y. and Hanover, G., "Cassini Spacecraft Attitude Control Flight Performance," AIAA-2005-6269, Proceedings of the AIAA Guidance, Navigation, and Control Conference, San Francisco, California, 15–18 August 2005.
2. Macala, G. A., "Design of the Reaction Wheel Attitude Control System for the Cassini Spacecraft," AAS Paper 02-121, 27–30 January 2002.
3. Emily Pilinski and Lee, A.Y., "Pointing Stability Performance of the Cassini Spacecraft," *Journal of Spacecraft and Rockets*, Volume 46, No. 5, September-October, 2009, pp. 1007–1015.
4. Meakin, P.C., "Cassini Attitude Control Fault Protection: Launch to End of Prime Mission Performance," Paper AIAA-2008-6809, Proceedings of the AIAA Guidance, Navigation, and Control Conference, Honolulu, Hawaii, 18–21 August 2008.
5. Robertson, B. and Stoneking, E., "Satellite GN&C Anomaly Trend," Paper AAS 03-071, 26th Annual AAS Guidance and Control Conference, Breckenridge, Colorado, 5–9 February 2003.
6. Dahl, P.R., "Measurement of Solid Friction Parameters of Ball Bearings," The Aerospace Corporation, Report No. SAMSO-TR-77-132, March 10, 1977.
7. Harris, T.A., *Rolling Bearing Analysis*, John Wiley & Sons, Inc., 4th edition, 2001.
8. Hamrock, B.J., *Fundamental of Fluid Film Lubrication*, McGraw-Hill, New York, 1994.
9. Bhushan, B., *Introduction to Tribology*, John Wiley and Sons, Inc., 2002.
10. Nelder, J. A. and Mead, R. A., "Simplex Method for Function Minimization," *Computer Journal*, Vol. 7, No. 4, 1965, pp. 308-313.
11. Kannel, J.W. and Snediker, D.K., "Hidden Cause of Bearing Failure," *Machine Design*, Vol. 49, Issue 8, April 7, 1977, pp. 78–82.
12. Shapiro, W., Murray, F., Howarth, R., and Fusaro, R., "Space Mechanisms Lessons Learned Study, Volume II – Literature Review," NASA Technical Memorandum 107047, NASA Lewis Research Center, September 1995.
13. Tungseth, A.E., "DSP Wheel Recent Experience," Proceedings of the 17th Annual AAS Rocky Mountain Guidance and Control Conference, Keystone, Colorado, 2–6 February 1994, pp. 593–606.
14. Stevens, K.T., "Experimental Observations on Torque Variation Caused By Ball Bearing Cage Instability," Proceedings of Second Space Tribology Workshop, ESTL, UK, 15–17 October 1980.
15. Loewenthal, S., Boesinger, E.A., and Donley, A.D., "Observations of Cage Instability," Proceedings of the DOD/Instrument Bearing Working Group, 1991.
16. Kirsch, M. G. F., Martin, J., Pantaleoni, M., Southworth, R.T., Schmidt, F., Webert, D., and Weissmann, U., "Cage instability of XMM-Newton's Reaction Wheels Discovered During the Development of an Early Degradation Warning System," Paper 1,275,204, Proceedings of the SpaceOps 2012, Stockholm, Sweden, 11–15 June 2012.
17. Cliff Lee and Allan Y. Lee, "Cassini Reaction Wheel Momentum Bias Optimization Tool," AIAA-2005-6271, Proceedings of the AIAA Guidance, Navigation, and Control Conference, San Francisco, California, 15–18 August 2005.
18. Mittelsteadt, C. O., "Cassini Attitude Control Operations – Guidelines Levied on Science To Extend Reaction Wheel Life," AIAA Guidance, Navigation, and Control Conference, AIAA, Washington, DC, 2011.
19. Roberts, B. A., Kruk, J. W., Ake, T. B., Englar, T. S., Class, B. F., and Rovner, D. M., "Three-axis Attitude Control with Two Reaction Wheels and Magnetic Torquer Bars," AIAA Guidance, Navigation, and Control Conference, AIAA, Washington, DC, 2004.
20. Dellinger, W.F., and Shapiro, H.S., "Attitude Control on Two Wheels and No Gyros – The Past, Present, and Future of the TIMED Spacecraft," AIAA/AAS Astrodynamics Specialist Conference, AIAA, Washington, DC, 2008.
21. Kuninaka, H. and Kawaguchi, J., "Deep Space Flight of Hayabusa Asteroid Explorer," Proceedings of SPIE, Vol. 6960, Paper 696,002, 2008.
22. Bruno, D., "Contingency Mixed Actuator Controller Implementation for the Dawn Asteroid Rendezvous Spacecraft," Paper AIAA-2012-5289, AIAA Space 2012 Conference and Exposition, Pasadena, California, 11–13 September 2012.

23. Macala, G.A., Lee, A.Y., and Wang, E.K., "Feasibility Study of Two Candidate Reaction Wheel/Thruster Hybrid Control Architecture Designs for the Cassini Spacecraft," AIAA-2012-4541, Proceedings of the AIAA Guidance, Navigation, and Control Conference, Minneapolis, Minnesota, 13–16 August 2012.